©2011 Society of Economic Geologists, Inc.
Economic Geology, v. 106, pp. 835–867

The Sandstone-Hosted Beverley Uranium Deposit, Lake Frome Basin, South Australia: Mineralogy, Geochemistry, and a Time-Constrained Model for Its Genesis*

Pierre-Alain Wülser,[1,4,5,†] Joël Brugger,[1,2] John Foden,[1] and Hans-Rudolf Pfeifer[3]

[1] *CRC LEME and Tectonics, Resources and Exploration (TRaX), School of Earth and Environmental Sciences, University of Adelaide, Adelaide, SA 5005, Australia*

[2] *Division of Minerals, South Australian Museum, North Terrace, SA 5005, Australia*

[3] *Centre d'Analyse Minérale, Université de Lausanne, Anthropole, CH-1015 Lausanne, Switzerland*

[4] *Afmeco Mining and Exploration Pty Ltd (AREVA NC), 80 Leader Street, Forestville, WA 5035, Australia*

[5] *AUSTRALP SARL, Casepostale 72, CH-1292 Chambésy, Switzerland*

Abstract

The sandstone-hosted Beverley uranium deposit is located in terrestrial sediments in the Lake Frome basin in the North Flinders Ranges, South Australia. The deposit is 13 km from the U-rich Mesoproterozoic basement of the Mount Painter inlier, which is being uplifted 100 to 200 m above the basin by neotectonic activity that probably initiated in the early Pliocene.

The mineralization was deposited mainly in organic matter-poor Miocene lacustrine sands and partly in the underlying reductive strata comprising organic matter-rich clays and silts. The bulk of the mineralization consists of coffinite and/or uraninite nodules, growing around Co-rich pyrite with an S isotope composition ($\delta^{34}S$ = 1.0 ± 0.3‰), suggestive of an early diagenetic lacustrine origin. In contrast, authigenic sulfides in the bulk of the sediments have a negative S isotope signature ($\delta^{34}S$ ranges from −26.2 to −35.5‰), indicative of an origin via bacterially mediated sulfate reduction. Minor amounts of Zn-bearing native copper and native lead also support the presence of specific, reducing microenvironments in the ore zone. Small amounts of carnotite are associated with the coffinite ore and also occur beneath a paleosoil horizon overlying the uranium deposit.

Provenance studies suggest that the host Miocene sediments were derived from the reworking of Early Cretaceous glacial or glaciolacustrine sediments ultimately derived from Paleozoic terranes in eastern Australia. In contrast, the overlying Pliocene strata were in part derived from the Mesoproterozoic basement inlier. Mass-balance and geochemical data confirm that granites of the Mount Painter domain were the ultimate source of U and REE at Beverley. U-Pb dating of coffinite and carnotite suggest that the U mineralization is Pliocene (6.7–3.4 Ma).

The suitability of the Beverley deposit for efficient mining via in situ leaching, and hence its economic value, are determined by the nature of the hosting sand unit, which provides the permeability and low reactivity required for high fluid flow and low chemical consumption. These favorable sedimentologic and geometrical features result from a complex conjunction of factors, including deposition in lacustrine shore environment, reworking of angular sands of glacial origin, deep Pliocene weathering, and proximity to an active fault exposing extremely U rich rocks.

Introduction and Location

The Beverley uranium deposit is located in the eastern piedmont flanking the North Flinders Ranges toward Lake Frome. It lies approximately 13 km away from the exposed crystalline basement of the Mount Painter inlier (Fig. 1), in the Paralana High Plains, a piedmont terrace that lies directly at the eastern foot of the much steeper topography of the basement inlier. The deposit was discovered in November 1969 by the Transoil-Petromin Group, making it the first sandstone-hosted uranium deposit in Australia. Regional prospecting in the Cenozoic sediments of the Lake Frome basin resulted in the discovery of additional uranium occurrences and deposits (e.g., Honeymoon-East Kalkaroo, Gould's Dam, and Oban). In November 2000, after 25 years of tribulations, extraction of uranium commenced at the Beverley deposit using in situ acid-leaching techniques, the first such operation in Australia. By December 2010, Heathgate Resources Pty. Ltd. had produced ~7,400 metric tons (t), with remaining reserves estimated at ~10,000 t of U_3O_8 at a grade of 0.25 percent U_3O_8 (Heathgate Resources Pty Ltd). The in situ acid-leaching techniques method uses an acidic, oxidizing (H_2SO_4-O_2) liquor to extract U from the permeable, unreactive sediments. Recent exploration in the immediate vicinity of Beverley has led to the discovery in 2005 of a new mineralized zone to the west of the mine: the Four Mile deposits (Fig. 1b).

The genesis of the Beverley deposit remains a source of debate. Previous authors classify the deposit among the paleochannel-hosted roll-front type (Callen, 1975; Haynes, 1975; Curtis et al., 1990). However, the nature of the paleochannel remains controversial, and Haynes (1975) stated that the Beverley Sands could not only be stream channels, scour channels, or outwash plains, but also sand dunes. The map of the underlying Alpha Mudstone surface around the Beverley deposit (McConachy et al., 2006) is reminiscent of a paleoshoreline with curved beaches. The proposed uranium sources for the deposit include: (1) the Mount Painter domain basement, (2) the Miocene formations themselves, or (3) the alluvial fans of the Willawortina Formation (Callen, 1975; Haynes, 1975; Hochman and Ypma, 1987), though

† Corresponding author: e-mail, pierre-alain@wulser.com
*Appendix Tables D1–D4 follow the references.

0361-0128/11/3970/835-33

Submitted: January 10, 2010
Accepted: March 12, 2011

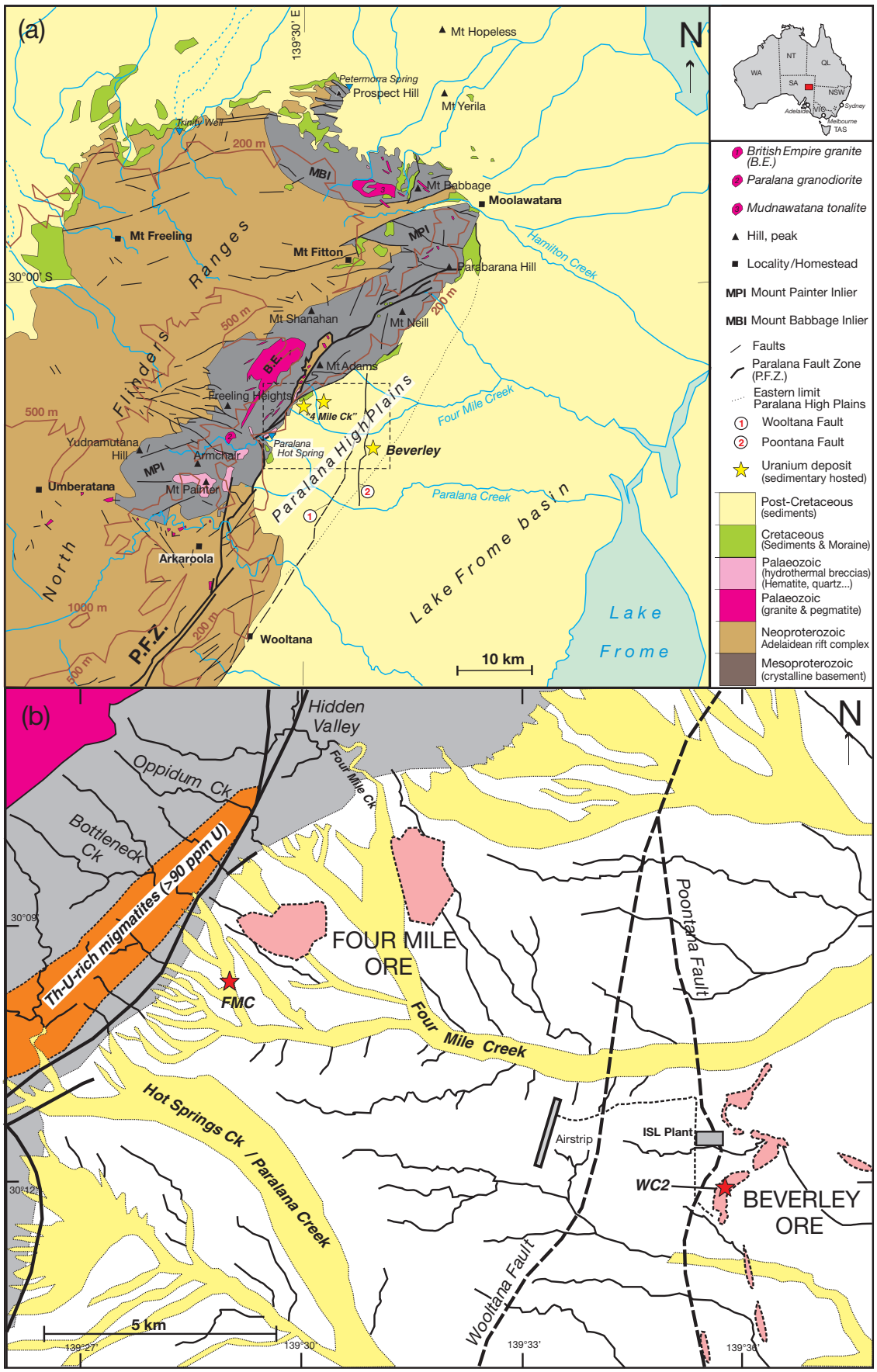
(a)
N
139°30' E
Mt Hopeless
Petermorra Spring
Prospect Hill
Mt Yerila
Trinity Well
200 m
MBI
Mt Babbage
Moolawatana
Mt Freeling
Mt Fitton
MPI
Parabarana Hill
Hamilton Creek
30°00' S
Flinders Ranges
500 m
Mt Shanahan
Mt Neill
200 m
B.E.
Mt Adams
Freeling Heights
"4 Mile Ck"
Paralana High Plains
Four Mile Creek
500 m
Yudnamutana Hill
Armchair
Paralana Hot Spring
Beverley
MPI
Umberatana
Mt Painter
Paralana Creek
Arkaroola
North
Lake Frome basin
1000 m
P.F.Z.
200 m
Wooltana
Lake Frome
500 m
10 km
NT
QL
WA
SA
NSW
Sydney
Adelaide
Melbourne
TAS
British Empire granite (B.E.)
Paralana granodiorite
Mudnawatana tonalite
Hill, peak
Locality/Homestead
MPI Mount Painter Inlier
MBI Mount Babbage Inlier
Faults
Paralana Fault Zone (P.F.Z.)
Eastern limit Paralana High Plains
Wooltana Fault
Poontana Fault
Uranium deposit (sedimentary hosted)
Post-Cretaceous (sediments)
Cretaceous (Sediments & Moraine)
Palaeozoic (hydrothermal breccias) (Hematite, quartz...)
Palaeozoic (granite & pegmatite)
Neoproterozoic Adelaidean rift complex
Mesoproterozoic (crystalline basement)
(b)
N
Hidden Valley
Oppidum Ck
Four Mile ck
Bottleneck Ck
Th-U-rich migmatites (>90 ppm U)
30°09'
FOUR MILE ORE
Poontana Fault
FMC
Four Mile Creek
Hot Springs Ck / Paralana Creek
Airstrip
ISL Plant
WC2
BEVERLEY ORE
30°12'
Wooltana Fault
5 km
139°27'
139°30'
139°33'
139°36'

most authors favor the Mount Painter domain as the most likely source. Dating of secondary uranium minerals resulting from the weathering of basement mineralizations in the Mount Painter domain demonstrates the recent mobility of uranium (Elburg et al., 2003) and groundwaters containing uranium concentrations up to 1 ppm exist in the U-rich Mesoproterozoic gneisses (Brugger et al., 2005). Studies of the quartz thermoluminescence in the Beverley Sands unit and the adjacent units (Hochman and Ypma, 1987) revealed that the Beverley Sands were exposed to, or still are in contact with, a radioactive source up to 4 km to the west of the uranium mineralization. Hochman and Ypma (1987) also revealed that the under- and overlying sand formations lacked the thermoluminescence of the Beverley Sands unit, reinforcing the interpretation of the Beverley Sands as a confined aquifer channeling the uraniferous groundwater.

Based mainly on the study of the mineralogy and geochemistry of the ore minerals and the hosting and surrounding sediments, this paper aims to elucidate the genesis of the Beverley deposit in its geologic framework. In particular, a detailed study of the heavy mineral populations in the sediments, including zircon typology, age distribution, and geochemistry, sheds light on the mineralization process, as well as on tectonic activity and sediment sources. We provide the first U-Pb data on authigenic minerals to constrain the timing of uranium mineralization in the Lake Frome basin. We also review some geologic features of the Mount Painter domain to constrain the sources of uranium and ore fluids. The recent tectonic activity in the North Flinders Ranges (neotectonics) and the formation of the successive sedimentary basins are discussed in regard to their role in mobilizing uranium. This work fills a gap in the literature on uranium deposits in South Australia, since no extensive study of Beverley-type mineralization is available; this study also provides new ideas and tools for the study and exploration of sandstone-hosted uranium deposits.

Geologic Setting

General geology

The Mount Painter and the Mount Babbage inliers in the northern tail of the Flinders Ranges are two tectonic windows into the underlying crystalline Proterozoic basement of the Adelaide geosyncline or Adelaide Rift Complex (Fig. 1a). These inliers are together named the Mout Painter domain (Brugger et al., 2005). The major active Paralana fault zone defines the domain's eastern border. The Paralana fault zone is a cluster of faults with a general northeast-southwest trend (Fig. 1). The basement rocks in the Mount Painter domain are Mesoproterozoic and not older than ~1590 Ma (Fanning et al., 2003). The granitoids of the Mount Painter domain are unusually rich in uranium and thorium, with localized metasomatic enrichments reaching ~100 ppm U at kilometer scale (e.g., Neumann et al., 2000). Numerous primary uranium occurrences are widespread throughout the basement rocks (Coats and Blissett, 1971; Brugger et al., 2004, 2011). The Mount Painter domain represents the northeast corner of the Curnamona province. Most parts of the Curnamona province are covered by rift-related volcano-sedimentary sequences deposited from the Neoproterozoic (~830 Ma) to the Cambrian. In the Adelaide geosyncline, this sedimentation was terminated by the onset of the Delamerian orogeny (514–490 Ma; Foden et al., 2006). During this orogen the Mesoproterozoic basement and the volcano-sedimentary rift sequences were subjected to metamorphism and deformation reaching amphibolite facies in most of the Mount Painter domain (Sandiford et al., 1998). Delamerian magmatism in the Mount Painter domain is restricted to pegmatite and small leucogranite intrusions. A second period of felsic magmatism took place after the end of the Delamerian at ~440 Ma (Mudnawatana tonalite, Paralana granodiorite, and British Empire granite; Fig. 1; Elburg et al., 2003). The Lake Frome basin lies directly to the east and north of the Mount Painter domain. It hosts a thick sequence of sediments that were deposited in a number of sub-basins. For the most part, the stratigraphic record in these basins extends up from the Cretaceous (Eromanga basin), which lays unconformably on both Adelaidean and Mount Painter domain basement rocks. The Beverley deposit is hosted in Miocene formations within the Lake Frome basin, which belong to the Callabonna sub-basin, part of the larger Lake Eyre basin.

Cretaceous: The basal strata in both the Lake Frome and Lake Eyre basins are Lower Cretaceous formations (Fig. 2; Cadna-owie Formation) and onlap the Mount Painter domain and the Adelaide Rift Complex (Parabaranna Sandstone; Krieg et al., 1995). These formations are mainly composed of quartz-rich sandstones to conglomerates with quartzite and quartz pebbles. The presence of glacial diamictite at the base of the Cadna-owie Formation, west of the Petermorra Springs at Trinity Well (Fig. 1) is the first definitive evidence for an Early Cretaceous glaciation (Alley and Frakes, 2003), for which palynology data give ages ranging from Berriasian to Valanginian (144–131 Ma). Paleolatitudes around the North Flinders Ranges were ~66° S during the Lower Cretaceous (Veevers, 2006). The postglacial environment of deposition was fluviatile, with the area bordering the North Flinders Ranges forming the edge of the basin. The widespread deposition of the Aptian Bulldog Shale marked a change to marine conditions (Fig. 2). The Bulldog Shale is overlain by the tidal to intertidal Coorikiana Sandstone (Krieg et al., 1995). The Upper Cretaceous sedimentation in the Eromanga basin (Winton Formation) consists of nonmarine shales, siltstones, and sandstone with minor coal layers (Krieg

FIG. 1. Regional geology of the Mount Painter domain and location of the Beverley deposit. (a) The Paralana fault zone (PFZ) delineates the northwest border of the Curnamona province. This simplified geologic map underlines the major discontinuities: Neoproterozoic (~830 Ma), Cambro-Ordovician (Delamerian orogeny), Cretaceous glaciation and sedimentation. Cretaceous formations are widespread on and around the inliers, under 250-m elev. Inset: location of the study area. The 200-, 500-, and 1,000-m elev lines are also displayed. (b). The outlines of the Beverley and Four Mile uranium deposits are displayed in pink; red stars represent the samples used in this study (Four Mile Creek stream sediments and WC2 core). The REE-Th-U–rich migmatitic gneisses are indicated in orange, immediately to the west of the Paralana fault system. Additional regional faults are also reported (Poontana, Wooltana faults).

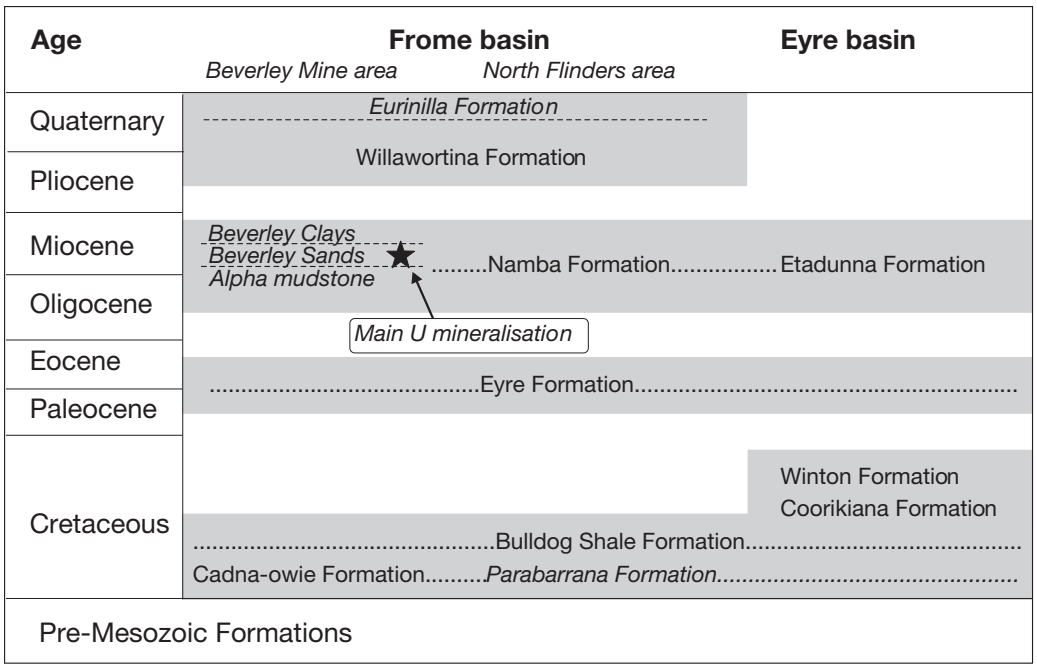

FIG. 2. Regional lithostratigraphy for the Mesozoic and Cainozoic units. The age limits are drawn approximately and discussed in the text. The main uranium mineralization at Beverley is located in a sandy unit: the Beverley Sands. Formations reported in italics are restricted to localized areas.

et al., 1995). Although this formation has not been described in the southern part of the basin, we mention it here because it generally forms the substrate of the following Cainozoic sediments. The final stage of the Upper Cretaceous was dominated by erosion and weathering. Cretaceous formations are preserved to the west of Beverley. Some outcrops in the Four Mile Creek bed and next to the ranges have been recognized as Upper Cretaceous members (Campana et al., 1961a, b) and recently dated to Early Cretaceous (Stoian, 2010). The Four Mile West uranium deposit is hosted by Early Cretaceous sandstones (Stoian, 2010).

Paleocene to Oligocene: Following a ~30 to 50 Ma period of weathering and erosion, the sedimentary record restarts in the Lake Eyre basin during the late Paleocene (Wopfner et al., 1974; Callen et al., 1995a; Stoian, 2010). Above this, the Paleocene to Eocene Eyre Formation is widespread, being present west, north, and east of the North Flinders Ranges. The Callabonna sub-basin (Lake Frome area) and the Torrens basin (Lake Torrens area) may have been separated by a high during the Eocene, although potential remnants of Eocene sediments are recognized between the two basins overlying Adelaide geosyncline series rocks (Coats, 1973). The Eyre Formation is composed mostly of carbonaceous pyritic mature sands, locally intercalated with clay and gravel beds (Wopfner et al., 1974), deposited in braided rivers during the initial stages of uplift of the North Flinders and the Olary Ranges and synchronous subsidence of the Lake Eyre basin (Callen et al., 1995a). Evidence of active faulting and uplift during the Eocene is recorded by fission-track ages around the Paralana fault zone, east of the Paralana High Plains, and Beverley (Foster et al., 1994; Mitchell et al., 2002). The Eocene Eyre Formation is host to the Four Mile East uranium deposit (Stoian, 2010).

Late Oligocene to Miocene: Sedimentation during the Miocene continued in lacustrine, alluvial environments, depositing the Etadunna and the Namba Formations. The latter hosts the Beverley uranium deposit. In the vicinity of present-day Lake Eyre, these sediments are calcareous and dolomitic, grading up to green and gray Mg-rich claystone and fine sand, and are partly derived from reworking of the underlying Eyre Formation (Callen et al., 1995a). The Namba Formation in the Callabonna sub-basin is composed of angular, immature sands and silts, black smectite-rich partly magnesian clay and dolomite. The sequence of sediments thickens westward toward the Flinders Ranges. These Miocene sediments contain elements reworked from the underlying Cretaceous to Eocene rocks. At Beverley, three Namba subunits are defined: (1) the Alpha Mudstone, (2) the mineralized Beverley Sands, incised in the Alpha Mudstone, and (3) the Beverley Clays, forming an aquaclude cap over the mineralized Beverley Sands (Fig. 2). The age of the Beverley Clays is unclear. The depocenter of the Namba Formation is located on the eastern part of the basin, south of the Beverley mine, and the formation is thickest (90–170 m) near the shores of Lake Frome, but the age of the Namba Formation deposition extends from the late Oligocene to the Pliocene in the Wooltana 1 drill hole (Martin, 1990).

Pliocene to Quaternary: The Namba Formation is locally capped by a silicic or ferruginous duricrust in the Lake Frome area. The upper layers of the formation contain kaolinite, alunite, and gypsum; this mineral association is interpreted to result from the same weathering event that formed the duricrust (Callen and Tedford, 1976; Benbow et al., 1995). The age of this weathering has been interpreted by these authors to be late Pliocene. During the Pliocene, the Curnamona province was tectonically active, and its western margin was

being displaced by normal and transcurrent (or transpressive) faulting. This uplifted the western margin, producing the current 100 to 200 m of relief and forming the sharp eastern escarpment of the North Flinders Ranges (Mt. Neill and Mt. Adams), as well as the Paralana High Plains. The Beverley deposit is located along the eastern side of the Paralana High Plains, close and to the east side of the Poontana and Wooltana fault zones (Fig. 1b). Both this and the Mount Neill-Mount Adams blocks are tilted to the northwest. This tilt caused an eastward migration of the depositional center of the Lake Frome basin. Recent seismic lines across the area also indicate the presence of a "horst-like" structure as well as several major faults (Burtt et al., 2004).

Alluvial fans have and continue to build up a molasse foreland, which has formed a wide alluvial plain extending to the shores of the present-day Lakes Frome, Callabonna, and Blanche (Callen and Tedford, 1976; Callen et al., 1995b). The molassic Willawortina Formation (Fig. 2) is synchronous with the main uplift and unroofing of the Mount Painter domain and consists of coarse siliciclastics as well as fine sands and clays deposited in more distal lacustrine or facies. Paleomagnetic data on the Willawortina sediments and paleosoils around the Lake Frome area indicate that much of the formation is older than 780,000 years (Callen et al., 1995b). The current depositional environment around Beverley consists of alluvial fans and migrating fluvial channels and levees that form the Eurinilla Formation (Fig. 2), a clay-rich ferruginous resedimented conglomeratic soil formation with residual quartz lags (Callen et al., 1995b).

Background information on the uranium mineralization

Geometry, relationship to formations and regional faults: The initially published geometrical models of Beverley all described channel-type (Beverley sands) mineralization with a north-northeast–south-southwest orientation (Haynes, 1975), with the sand formations hosting the mineralization interpreted as paleodrainage channels in the underlying lacustrine Alpha Mudstone bedrock. Curtis et al. (1990) mentioned an oxidation interface with anomalous uranium traceable in the Namba Formation over an area of 25 × 15 km. Heathgate Resources defined the north and central-south ore zones, both with northeast-southwest trends, located immediately west of the Poontana fault in Miocene sands and in the lower faulted block. Faulting is interpreted to have been active during the Quaternary, as it affects the upper Willawortina Formation (Heathgate Resources Pty. Ltd., 1998). The extension of the Wooltana fault (SW) is also interpreted to project west of Beverley and the Poontana fault (Fig. 1). Based on paleosurface reconstruction using drill hole and airborne electromagnetic surveys, uranium mineralization is spatially linked to the edges of relief and depressions in the underlying mudstone (Marsland-Smith, 2005; McConachy et al., 2006). The mineralization does not form a classic "roll-front" geometry, but rather more sheets. This geometry is interpreted by both Marsland-Smith (2005) and McConachy et al. (2006) to result either from structural (faulting) or paleoenvironmental controls.

Mineralogy and geochemistry: Previous descriptions of the ore have identified little mineral diversity, only describing fine-grained uraninite (Haynes, 1975), coffinite and pyrite (Brunt, 1978; Curtis et al., 1990). Most of the Beverley (and Four Mile) mineralization occurs in organic matter-poor sands (J. Oram and A. Marsland-Smith, pers. commun.). Whole-rock analyses revealed a close correlation between elevated U concentrations and high Co, S, Bi, Pb, Co, Ni, Cu, and Cd with lesser Zn, light rare earth elements (LREE), and Y (Marsland-Smith, 2005). The chemistry of the retrieved in situ acid-leaching techniques acid solutions (i.e., after leaching) also provides qualitative information on the ore mineralogy; by comparing the solutions before and after reaction, taking into account mixing with the local groundwater (Heathgate Resources Pty. Ltd., 1998), a relative increase of 10^2 to 10^3 is measured for the concentrations of V, U, Ni, Se, Cd, and Al; 10^1 to10^2 for Co, Fe, As, and Cr, as well as minor (>3) relative increase in F and Pb.

Sampling and Methodology

WC2 drill core

The main part of this study has been conducted on the WC2 diamond core (30°11'55.3"S/139°35'48"E, 80 m), which is preserved and available at the Primary Industries and Resources South Australia (PIRSA) core library (Nr 137-058). Additional sediment samples were collected in the Paralana High Plains and in the neighboring crystalline basement. The WC2 core was drilled by Western Nuclear in the central ore zone of the Beverley deposit in February 1972, prior to any leaching test that could have affected the primary mineral assemblage and geochemistry. The WC2 drill hole also represents the type section for the Willawortina Formation (Callen and Tedford, 1976). WC2 is the only diamond core available through the Beverley deposit. The hole reached a length of 146.6 m, ending in the Alpha Mudstone (Namba Formation), but the available cored length extends from the surface down to 136 m. The recovery rate of the entire core was low (50%), especially in the Willawortina Formation; this however did not impact the results of this study, based on samples from selected intervals. We relogged the core (Fig. 3) and prepared samples for different analytical or separation techniques. Our observations are generally consistent with the clay mineralogy, texture, or sedimentary facies data of Callen (1975). In addition to the samples from the WC2 core, a large sample has been taken from a Four Mile Creek tributary 8 km upstream the Beverley uranium mine (FMC, Fig. 1b) to provide accurate information about the heavy mineral contents of the Four Mile catchment, the source area for the Willawortina Formation sediments.

Heavy mineral separation and sample preparation

Heavy minerals were extracted and concentrated from sediments or crushed rocks by manual panning and micro-jigging, and then were further separated by strong handheld permanent magnets. These simple tools were utilized to avoid possible cross contamination resulting from the use of heavy liquids and electromagnets. However, a possible contamination due to the drilling process and transportation to the storage is inevitable in the case of cored sediments. The recovered heavy mineral concentrates from the sand and silt fractions were first extracted at a mean bulk density of 3.0 g/cm^3 and separated by Fe-Nd-B–type magnets into

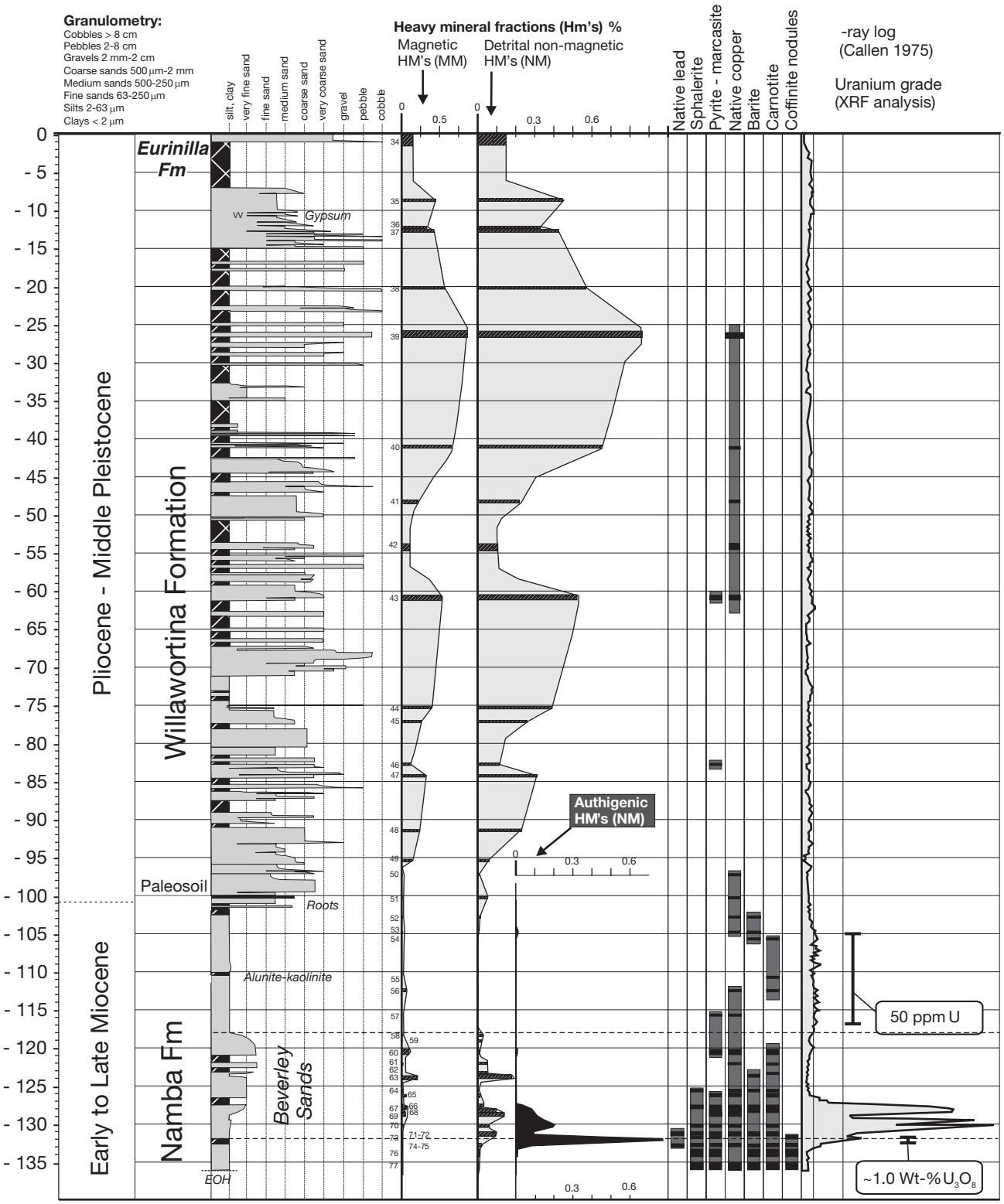

FIG. 3. WC2 drill core log with gamma, uranium grades, and heavy minerals assemblage. The heavy minerals have been represented on two logs: nonmagnetic (NM) and magnetic (MM). The authigenic minerals in the WC2 core are also shown and belong to the nonmagnetic fraction. A paleosoil with roots and oxidized cracks occurs between –100 and –102 m; it defines the unconformity between the Namba Formation and the beginning of the Willawortina Formation sedimentation, essentially debris flows. Only ~50 percent of the core was recovered, with lost intervals hatched on the granulometric log. The Namba Formation is formed of three units: the Beverley clays, the Beverley Sands, and the Alpha Mudstone at the bottom of the hole.

three fractions: ferromagnetic, paramagnetic, and nonmagnetic. The pulling force at the surface of the magnet was equivalent to 1.35 A of intensity on a Frantz isodynamic separator (calibrated on the 150-μm fraction). The non- and paramagnetic fractions were then separated into <4.0 and >4.0 g/cm^3 fractions, the latter being almost pure zircon-rutile-corundum. Minerals from concentrates were handpicked for typology (zircon), further analysis, or digital photography. Minerals selected for analysis, geochronology, or microscopy were mounted in epoxy resin disks and polished (final polish with ¼-μm diamond).

Zircon typology

Morphology-based zircon typology has been used as a tool to distinguish the nature of granites (Pupin, 1980) and to distinguish magmatic and inherited zircons in igneous rocks (e.g., Klötzli et al., 2001). Surface textures also provide information about the provenance of the grains (Cardona et al., 2005), and a combination of dating and typology can determine sedimentary provenances with better precision (Willner et al., 2003). Zircon typology is based upon the relative abundance of prisms and pyramids. Crystal forms have been divided into 64 main subtypes, corresponding to a unique combination of these crystal faces (Fig. 4a). Zircons from granitic rocks can be divided into eight main genetic typological subgroups; in these, the relative abundance of the prisms {100} and {110} is related to the temperature of crystallization. The typology of zircons extracted from sediments permits the definition of clusters of different origins; however, mixed populations and zircon grains that cannot be classified due to mechanical abrasion can complicate this analysis. In the current study, observations were made on zircon fractions using both electron and optical microscopy.

Chemical and isotopic analyses

The techniques used in this study include optical mineralogy, electron microscopy including backscattered electron imagery (BSEI) and energy-dispersive spectroscopy (EDS), electron microprobe (EMP) analysis (operating conditions and standards reported in Table 1), laser ablation inductively coupled plasma-mass spectrometry (LA ICP-MS), whole-rock X-ray fluorescence (XRF) spectrometry, and gas source stable isotope analysis for sulfur isotopes.

Sulfur isotope analyses were performed at the University of Lausanne, using a Carlo Erba 1108 elemental analyzer (EA) coupled to mass spectrometer (Finnigan Mat Delta S). The analytical uncertainty (2σ) was 0.2 per mil and data are reported as per mil (‰) deviations relative to the Canyon Diablo troilite (CDT) standard. Analyses were repeated two to three times when enough material was available and alternated regularly with international sulfide and sulfate standards. The sulfide analyses were performed on samples consisting of a few 10s to 100s of individual grains.

LA ICP-MS measurements were conducted at the Adelaide Microscopy Centre. The detailed technique and procedure used for zircon data was described in Reid et al. (2006), and only a summary of the acquisition parameters is provided here. Ablation was performed using the 213-nm radiation from a frequency quintupled Nd-YAG Adelaide geosyncline laser (holes ~40-μm diam). The ablated material was carried by an Ar-He gas medium into an Agilent 7,500-quadrupole ICP-MS. The data were corrected for instrument drift and the isotopic ratios calculated using the GLITTER software (Van Achterbergh et al., 1999). The following isotopes were measured: ^{204}Pb, ^{206}Pb, ^{207}Pb, ^{208}Pb, ^{232}Th, and ^{238}U. The standard used for calibration is a gem-quality red zircon, GJ: ^{207}Pb/ ^{206}Pb age is 608.5 ± 0.4 Ma, ^{206}Pb/^{238}U is 600.7 Ma, and ^{207}Pb/ ^{235}U is 602.2 Ma (Jackson et al., 2004) with undetectable ^{204}Pb with the used setup. Common lead correction was applied using the global second-stage Pb reservoir model of Stacey and Kramer (1975). For minerals devoid of ^{232}Th (e.g., carnotite), the correction was based on ^{208}Pb instead of ^{204}Pb (zircon and coffinite).

Trace elements in zircon were analyzed by LA ICP-MS at the J.W. Goethe-Universität, Frankfurt, using a Merchantek LUV213 ultraviolet Nd-YAG Adelaide geosyncline laser (213 nm) coupled with a Finnigan MAT ELEMENT II high-resolution ICP double-focusing mass spectrometer. The internal standard used was ^{29}Si, and the external standards used were NIST-610 glass and the 91500 zircon. Calibration problems occurred with REE-rich zircons, leading to saturation in signals for Y, Er, and Yb.

XRF whole-rock analyses were performed on a Philips PW2400 spectrometer at the Centre d'Analyse Minérale (CAM) at the University of Lausanne. Major elements were measured on $Li_2B_2O_4$ fused disks and minor and trace elements on pressed pellets. Ferrous iron was determined quantitatively by spectrophotometry using the Wilson's modified method (Wilson, 1960). A fraction of rock powder was dissolved in an H_2SO_4-HF mixture. Solutions were neutralized and buffered with H_3BO_4, and Fe^{2+} was complexed with 2,2'-bipyridine. The solutions were measured in the maximum range of absorption of the Fe^{2+} complex, and the FeO wt percent was calculated using a linear calibration based on five rock standards and a blank. REE and other trace elements were determined by LA ICP-MS on the fused disks, using an EXCIMER Laser (193 nm) coupled to an ICP-MS Perkin-Elmer ELAN 6100 DRC.

Heavy Minerals: Mineralogy and Provenance

The relative concentrations of the different heavy mineral fractions from WC2 drill core are listed in Table D1 and shown in Figure 3, together with the sedimentary and gamma-ray logs. Special attention has been given to the separation of the authigenic minerals from the detrital assemblages. The Willawortina and Namba Formations can be distinguished on the basis of their heavy mineral contents: the heavy mineral content of the Namba sediments does not exceed 0.4 wt percent, whereas the Willawortina Formation sediments nearly always carry more than 0.5 wt percent.

Detrital minerals populations

The alluvium from the Four Mile Creek sample has high heavy mineral contents (1–2 wt %), including U-, Th-, and REE-rich phases. Zircon, rutile, xenotime, monazite, polycrase, fergusonite, allanite, thorite, huttonite, and apatite are all abundant in these sediments. The Willawortina Formation sediments have a heavy mineral assemblage identical to the sediments of Four Mile Creek: they are rich in black magnetic minerals (ferrromagnetic; magnetite, ilmenite, hematite),

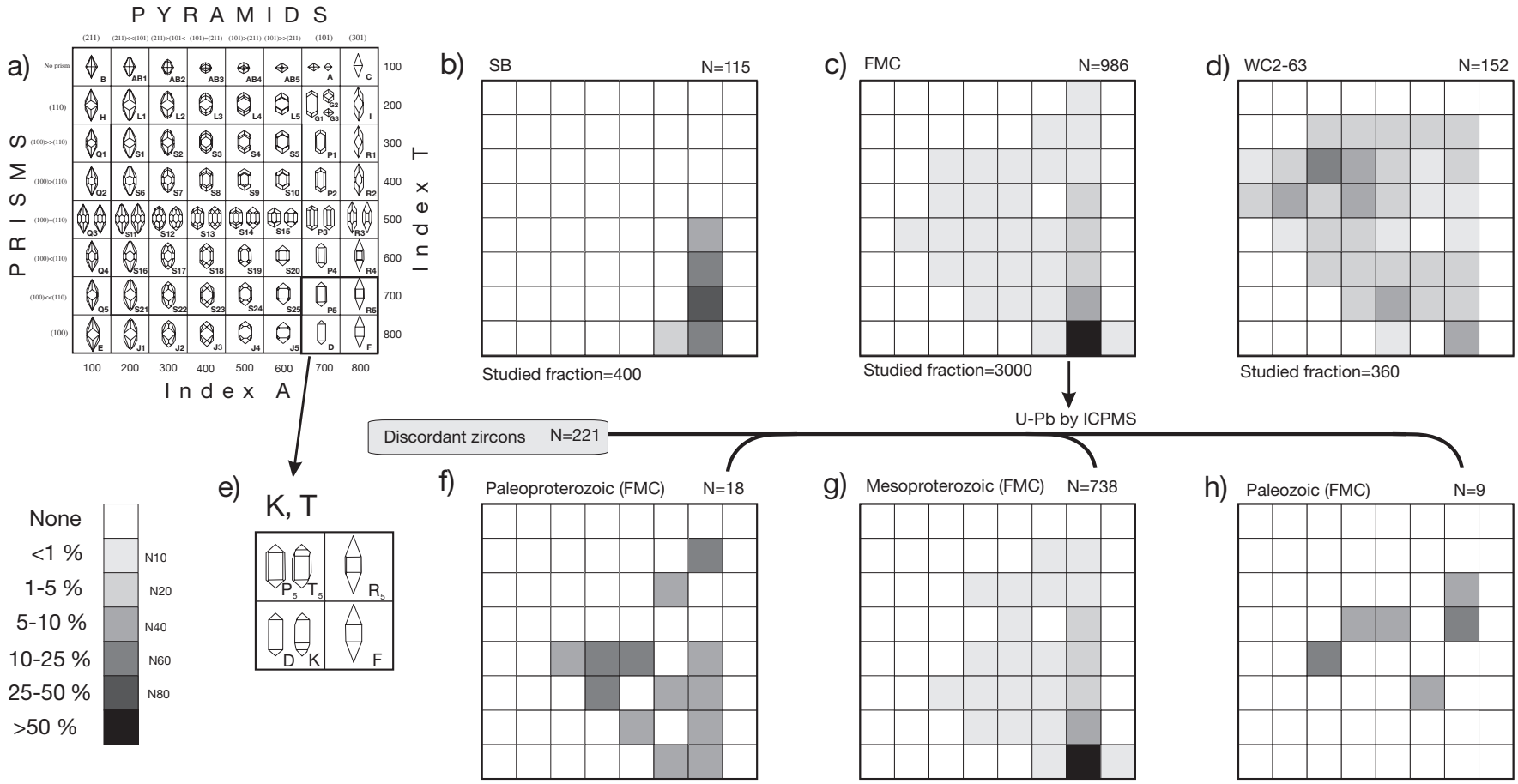

FIG. 4. Typological and geochronological populations of zircons in the WC2 core, Four Mile Creek, and SB creek source. (a). The typology grid of Pupin (1980) classification. Each unique combination of prisms and pyramids corresponds to a specific type, which is denominated by a letter and a number. Exceptions are zircons presenting "end-member" typologies (types A, B, C, D, E, F, G, H, I). Frequencies are reported in percents. N indicates the number of crystals plotted on the grid. Undetermined zircons are not part of this number. (b). SB sample is taken from a gully draining exclusively Mesoproterozoic granites. (c). Four Mile Creek is a large heavy mineral sample from a tributary of the Four Mile Creek, upstream of Beverley. (d). Zircons from the Beverley Sands unit. (e). Zoom in the bottom right corner of the typology grid with positioning of special types T5 and K in the P5 and D boxes. (f)-(g)-(h). As part of the characterization of the Mount Painter domain zircons, a representative part of the typology-determined zircons in Four Mile Creek were dated using U-Pb (LA-ICPMS). The Paleoproterozoic crystals show a dominance of S-types (metasedimentary basement units), whereas the Mesoproterozoic are D-P types (alkaline granites). A few Paleozoic zircons of S-P types are also reported (Paleozoic intrusions). Only a maximum of 10 to 12 percent of the zircons from the Beverley Sands could be sourced from the Mount Painter domain. A different sedimentary source containing S- and L-type zircons derived from peraluminous granites is required.

TABLE 1. EMPA Analytical Parameters, Analyzed Elements, and Standards

Coffinite, metals, and sulfide, carnotite
20 kV, 20 nA, spot size 1 μm

Line	Crystal	Standard	Interf cor.
MgK	TAP	Biotite	n/a
AlK	TAP	Biotite	n/a
SiK	TAP	Biotite	n/a
PK	PET	Apatite	Y
SK	PET	Marcasite	n/a
KK	PET	Biotite	U
CaK	PET	Apatite	n/a
VK	LIF	Rutile	Ti
FeK	LIF	Marcasite	n/a
CoK	LIF	Cobaltite	n/a
NiK	LIF	Pentlandite	n/a
CuK	LIF	Copper	Ba
ZnK	LIF	Zinc	U
AsL	TAP	Cobaltite	n/a
SeL	TAP	Selenium	n/a
MoL	PET	Molybdenite	n/a
PdL	PET	Palladium	n/a
CsL	PET	Pollucite	n/a
BaL	PET	Barite	Cu
PbM	PET	Lead	n/a
UM	PET	Uranium	n/a

Zircon, apatite, and xenotime
20 kV, 20 nA, spot size 1 μm

Line	Crystal	Standard	Interf cor.
FeK	LIF	Almandine	n/a
ErM	TAP	Erbium metal	n/a
YbM	TAP	Synthetic YbF_3	n/a
HfM	TAP	Cubic zirconia	n/a
CaK	PET	Almandine	n/a
ZrL	PET	Cubic zirconia	n/a
YL	PET	Cubic zirconia	n/a
PbM	PET	Crocoite	n/a
PK	PET	Apatite	Y
ThM	PET	Monazite	n/a
UM	PET	Uranium metal	n/a
AlK	TAP	Almandine	n/a
SiK	TAP	Olivine	n/a

Notes: All standards used from Astimex Scientific Ltd.; Sections METM25-44, REEM25-15, MINM25-53; Variable acquisition time on peak and background; CAMECA SX51, Adelaide Microscopy Centre

and also contain the paramagnetic minerals epidote, hornblende, garnet, xenotime, columbite, and monazite. The nonmagnetic assemblage is dominated by zircon and titanite, followed by rutile and corundum, anatase, sillimanite, tourmaline, fluorite, apatite, and topaz. Detrital sulfides (pyrite, chalcopyrite, galena, and molybdenite) are also present. Zircon grains are typically large, of brown, reddish, or black color, and cracked.

The Namba Formation has a clearly different heavy mineral assemblage. The upper Beverley Clays unit is poor in heavy mineral and dominated by rutile, with minor zircon, leucoxene, and corundum. Ferro- and paramagnetic minerals are rare. Monazite is present in minute amounts. Beneath the clays, the Beverley Sands unit contains zircon, minor rutile, anatase, and corundum. The zircons are different in color and morphology from those of the Willawortina population, consisting mainly of transparent and colorless crystals. The Alpha Mudstone is generally poor in heavy minerals and rutile is the dominant phase. The content of magnetic heavy minerals is extremely low compared to the Willawortina Formation. We evaluated the ratio of rutile (*ru*) to zircon (*zr*) in the different samples by grain counting. The $ru/(ru + zr)$ ratio varies between 1 to 3 in the Willawortina Formation, sharply increases (6–50) in the Beverley Clays, diminishes sharply in the Beverley Sands (0.1–0.7), and finally increases in the Alpha Mudstone (1–4; Table D1). The high proportion of zircon in the Beverley Sands' NM fraction suggests a different source, or different ratios of contributors, compared to the neighboring units. However, the Beverley Sands clearly contain an important contribution from a mature sedimentary source fed dominantly by granitic rocks. Zircons from the Beverley Sands also display some angular fractures and frequently present melt inclusions, indicating a felsic volcaniclastic origin (ignimbrites).

The distribution of corundum in the WC2 core is particularly interesting. This mineral, which is highly resistant to mechanical abrasion due to its hardness, is nearly absent from most of the Namba Formation. It starts occurring in significant amount at the level –106 m within 5 m of the top of the formation and remains abundant in the Willawortina Formation (Table D1). Corundum crystals are colorless, blue, less frequently black, and frequently bicolor.

Trace element chemistry of zircon

Trace elements were measured in 100 zircon grains from the heavy mineral concentrates at different levels in the WC2 core. The aim was to measure the uranium content of the zircons in order to check whether the zircons themselves could have played a role as a source for sandstone-hosted uranium mineralization and to use the trace elements signature as a means of differentiating provenance (e.g., Belousova et al., 2002). Zircon is a resistant refractory mineral that can incorporate many elements in its structure (e.g., P, Sc, Nb, Hf, Ti, U, Th, and REE). Zircon forms isostructural series with xenotime-(Y) (YPO_4) and all other xenotime-high rare earth element (HREE) members (Bea, 1996), as well as with coffinite ($USiO_4$) and hafnon ($HfSiO_4$). Most zircons grow in felsic magmas or high-grade metamorphic rocks, but some are hydrothermal. Mineral and/or melt partition coefficients are high for Hf, U, Th, Nb, Ta, heavy REE, Sc, and Y. Apart from U, these elements have low solubilities in hydrous fluids, hydrothermal zircons have low concentrations of these elements. Fluid-altered or hydrothermal zircons can contain hundreds of parts per million of other elements that are incompatible during igneous partitioning, for example, LREE, Sr, Ba, Ca, F, Fe, Mn, and Cu (Rubin et al., 1989). U- and Th-rich zircons become metamict with time; this causes swelling of the crystal structure and opening of microcracks, hence facilitating trace element incorporation and/or leaching via interaction with groundwater (Geisler et al., 2003).

Zircons with U/Th <6 probably originate from felsic magmas, but zircons with U/Th >6 are an unusual population from U-rich source rocks or are hydrothermally altered. The U and Th partitioning between the developing zircon and its surrounding felsic melt have been determined experimentally by Blundy and Wood (2003): $D_U^{(zircon/melt)}/D_{Th}^{(zircon/melt)} \approx 6$, with D_U varying from 97 to 130. Very limited experimental data give a $D_U/D_{Th}^{(zircon/melt)} \approx 3.5$ to 4.1 for granitic compositions at 20 kbars and 800° to 850°C (Rubatto and Hermann, 2007). Granitoids generally display Th/U between 5 and 2 but rarely less than 1. Zircon partitioning with $D_U/D_{Th} \approx 6$ results in a Th/U ratio in zircons between 1 and 2.

The distribution of U/Th values shows strong stratigraphic variation in the WC2 core, indicating changing sediment provenance (Table 2). The upper formation (Willawortina) has a much higher proportion of zircon with U/Th >6. Figure 5 illustrates the distribution of trace elements within these two zircon populations. Zircons with high U/Th are also Nb, Ta, HREE, and LREE rich. Tungsten, Sn, Mo, V, Cu, and Ti are also enriched in these zircons. The high U zircons display irregular chondrite-normalized curves with a positive tetrad effect, especially marked on the third tetrad (Gd-Ho). This feature is interpreted as the signature of hydrothermally altered zircons (Monecke et al., 2007). For many zircons, the $^{208}Pb/^{232}Th$ ratio displays a correlation between extremely high apparent ages (with a lot of common Pb) and high values of Nb, U, Sr, Ba, and REE. The presence of large incompatible elements, like Sr and Ba, can be linked to metamict and fluid-altered zircons that experienced a large degree of open-system behaviors; such zircons are unsuitable for U-Pb dating.

Zircon typology and regional sources

The trace element and geochronological data obtained from zircons from the Namba Formation in the WC2 core clearly indicate an origin distinct from the local basement inliers. Zircon typology has been applied to determine the sources of the sediments at the Beverley mine and its neighborhood. The zircons used for the typology study come from three different locations: (1) WC2-63, in the Beverley sands at the level –123.4 m; (2) FMC, Four Mile Creek stream sediments 8 km upstream the mine (Fig. 1); and (3) SB, a creek in the Babbage inlier draining Mesoproterozoic granites only.

The Four Mile Creek sample was selected because it represents a well-defined 12-km² watershed, which supplies a significant proportion of the Willawortina Formation. The watershed contains Mesoproterozoic quartzite and paragneisses (70%), Mesoproterozoic granites and orthogneisses (20%), and Paleozoic leucogranites and pegmatites (10%).

The bulk sediment sample from the Babbage inlier represents a watershed composed at more than 99 percent of Mesoproterozoic granites (Yerila and Terrapinna granites). Zircons from this sample display typologies typical of alkaline series granites. Some zircons display a rare typology with stocky, large prisms showing a dominance of {100} faces and a combination of {101} and {301} pyramids. This typology is restricted to high-temperature (~900°C) alkaline K-rich granites (Pupin, 1980). These zircons have fine cracks and are generally stained in black, brown, or orange. All these observations can largely be extended to the whole Mount Painter domain in which Mesoproterozoic granites abound. We base this argument upon additional observations made in heavy mineral separates from tens of crushed granites in the Mount Painter domain. These basement zircons are clustered around the D to P1 trend, generally centered on D or P5 (Fig. 4).

The typology of the zircons at Four Mile Creek was established on the basis of a population of ~3,000 grains. About 20 percent of the watershed surface consists of outcrops of Zr-rich (500–800 ppm) Mesoproterozoic granitoids, whereas about 10 percent are outcrops of Zr-poor (<80 ppm) Paleozoic intrusive rocks. The remaining part consists of Zr-poor quartzites (e.g., Mesoproterozoic Freeling Heights quartzites) that contain mainly rounded zircons on which no crystal faces are preserved. On this basis, it is not surprising to find only ~2 percent of Paleozoic zircons in the sample. The Paleozoic zircons of the Mount Painter domain are morphologically more complex than the Mesoproterozoic ones. They are colorless or milky crystals with inherited cores and

TABLE 2. Distribution of Zircons in WC2 Core According to Their Level and U/Th Value

Level		U/Th in zircon			
(m)	No.	< 0.75	0.75–1.49	1.50–5.9	> 6.0
–2	34		3	4	3
–9	35			5	5
–13	37		1	1	8
–20	38		1	5	2
–25	39		1	7	2
–42	40		5	2	3
–48	41	1		3	6
–75	44			9	1
–83	46		2	5	3
–84	47		5	5	
–97	50	2	6	1	1
–110	55		8	2	
–121	61		3	4	3
–126	64			8	2
–130	70	1	3	3	3
Th/U rock[1]		> 8	8–4	4–1	< 1

[1] For igneous zircon, implying $D_U/D_{Th(zircon/melt)} \approx 6$

FIG. 5. Diagrams of trace elements in zircons from the WC2 core. (a). Zircons have been divided into two categories using U/Th ratio = 6.0. Zircons with U/Th >6 are represented as black diamonds in all diagrams; they are related to a U-enriched magmatic rock or to a postcrystallization hydrothermal enrichment. (b). Nb/Ta diagram with the field of granitoids as defined by Belousova et al. (2002) for igneous zircons. (c). Most U-rich zircons also have high REE. (d). U-rich zircons also display REE tetrad effect, which is probably related to fluid alteration. (e). Zircons which have high Ta (outside of the granitoid field in (b)) have Mo and Sn enrichment, which indicates a relationship to S-type peraluminous granites or pegmatites. (f)-(i) Similar patterns can be found for W, Ti, V, and Cu.

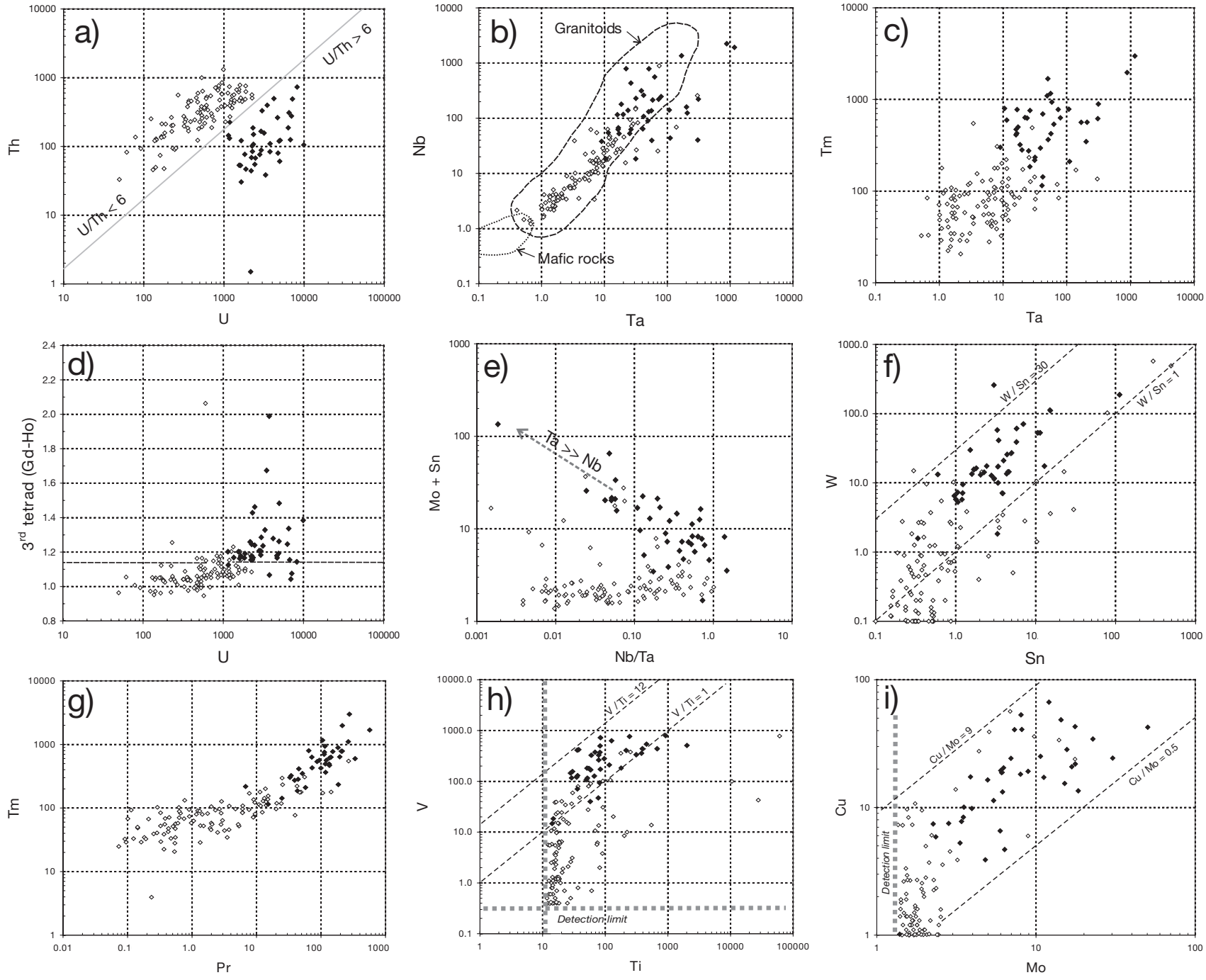
a)
U/Th > 6
U/Th < 6
Th
U
b)
Granitoids
Mafic rocks
Nb
Ta
c)
Tm
Ta
d)
3rd tetrad (Gd-Ho)
U
e)
Ta >> Nb
Mo + Sn
Nb/Ta
f)
W / Sn = 30
W / Sn = 1
W
Sn
g)
Tm
Pr
h)
V / Ti = 12
V / Ti = 1
Detection limit
V
Ti
i)
Cu / Mo = 9
Cu / Mo = 0.5
Detection limit
Cu
Mo

magmatic overgrowths (Neumann, 1996), which contrast with the orange to brown zircons originating from the local Mesoproterozoic granites.

Zircons separated from the Beverley Sands unit contain an unusual population of clear euhedral zircons exempt of any mechanical rounding. Typologies show a mixture of diverse populations (Fig. 4d). S-type zircons are dominant with a minor (10–12%) D- to P3-type population correlated to local inliers (Mount Painter domain) like in the Four Mile Creek. These S-type zircons are derived from S- or I-type granitoids. This is especially evidenced by the presence of numerous L-type zircons, which are only found in peraluminous granites. The source of these zircons is to be found outside the Mount Painter domain. We also observed some melt inclusions in freshly cracked zircons, indicating felsic volcanic origins for some of them at least. Detailed typology has been reported with the geochronological data in Table D2.

U-Pb zircon data

U-Pb data were obtained by LA ICP-MS on selected zircons from the Four Mile Creek and from the Beverley Sands (level −123.4 m). Ages are reported with 2σ errors (Fig. 6, Table D2). For the Four Mile Creek sample, a representative subset of zircons with P3 to D morphology and all other typologies was picked from a total of 3,000 zircons. This approach was chosen because Mesoproterozoic granites of the Mount Painter domain were recognized early on to display the typology D to P3, and we decided to study systematically all zircons with different typologies to unveil minor populations without having to date 3,000 zircons in a single sample. The original typology grid (Fig. 4c) is split into three diagrams based on ages: Paleoproterozoic, Mesoproterozoic, and Paleozoic (Fig. 4f-h). A population of S-type zircons, centered on S13 (Fig. 4f) and dated around 1640 to 1730 Ma can be interpreted to be sourced from calc-alkaline granites. Not surprisingly, most zircons are Mesoproterozoic (~1560 Ma) and plot on a discordia line with an approximate lower intercept of 100 to 250 Ma. The youngest concordant zircon is ~460 Ma.

The zircons from the Beverley Sands were handpicked for the determination of the typology (Fig. 4d), and a selection was dated. Special attention was given to zircons with crystalline faces and free of mechanical wear. A total of 152 grains out of 360 were typologically determined and a subset of 48 dated. Seventy percent of analyzed crystals gave concordant ages. Three major age groups are present: (1) Cretaceous-Jurassic zircons (24%), (2) Permo-carboniferous zircons (56%), and (3) Ordovician to Devonian (20%). The youngest analyzed zircon has an age of 130 ± 2.5 Ma.

Authigenic Minerals

Native elements: Copper, copper-zinc alloys, native lead

Authigenic native copper is common throughout the drilled length of the Namba Formation but also rarely appears in the Willawortina Formation. The native copper appears bright red, with a metallic luster. Some of these metallic grains are dendritic or spongy, which clearly indicates an authigenic origin. Cuprite (Cu_2O), tenorite (CuO), and a copper sulfide sometimes coat the grains. Lead is also detected by EDS on

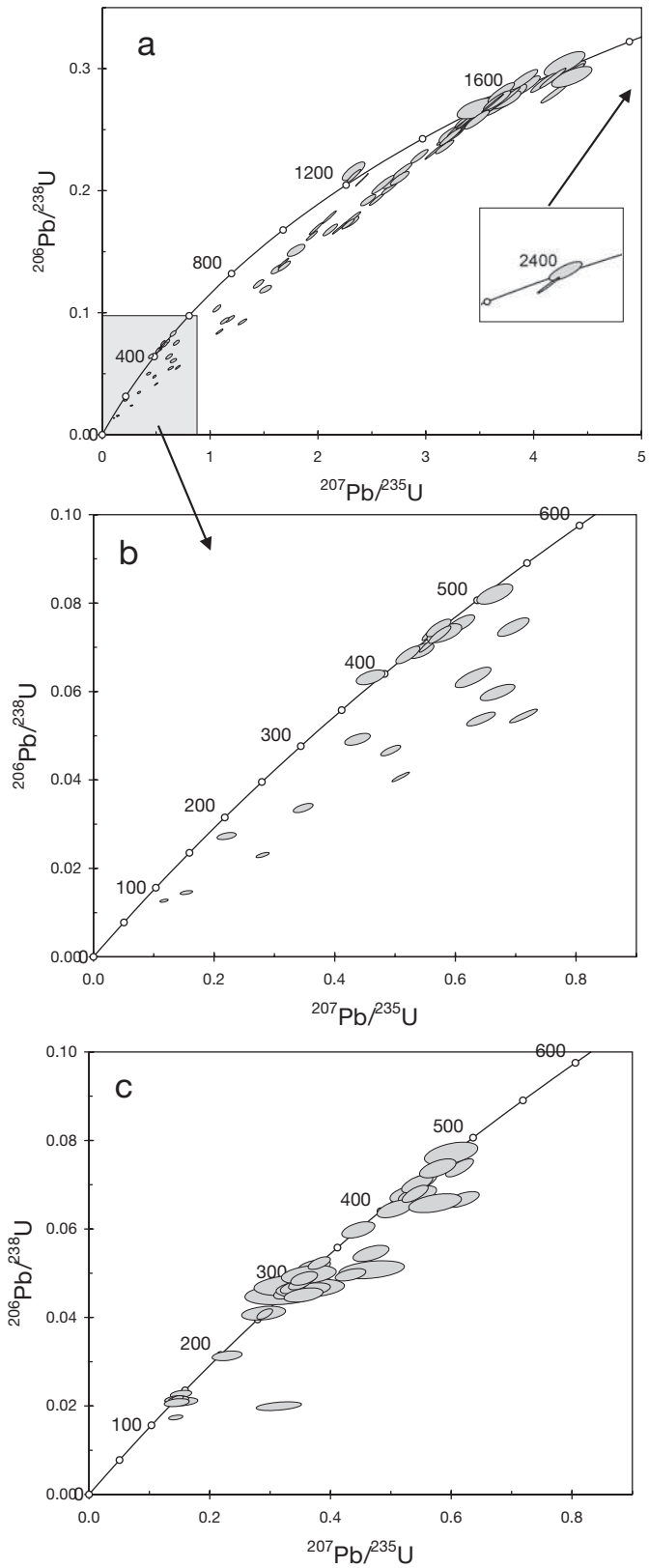

FIG. 6. U-Pb Concordia diagram of (a)-(b) Four Mile Creek zircons (FMC) and (c) Beverley sands zircons (WC2-63). In the Beverley Sands, the major age cluster is Permo-Carboniferous and indicates a sedimentary provenance from eastern Australia. The youngest zircon is 130 Ma; in contrast, the youngest concordant zircon in FMC is older than 400 Ma.

some of the grain rims. Electron microprobe analyses show that native copper grains contain variable proportions of Zn, with most of the grains having Zn <2 wt percent. A few grains of golden color have Zn-rich compositions close to Cu_2Zn (empirical formula $Cu_{1.97}Zn_{1.03}$). A contamination by a man-made alloy is unlikely, because of the association with an extensive Cu-Zn composition range. At a regional scale, native copper has been found at the basis of the Tertiary sediments on the Benagerie Ridge at the Kalkaroo prospect and in some hard-rock copper prospects and old mines of the Mount Painter domain (Noble et al., 1983). Native copper is also widespread at the basement-sediments interface of the eastern side of the Frome Lake (Burtt et al., 2004). A phase with Cu_2Zn composition (informal name tongxinite) was reported from gold-bearing quartz-carbonate veins in Transcaucasia and Southern Urals (Russia; Novgorodova et al., 1980), from silicified zones in a porphyry copper deposit (Yulong ore district, Tibet), and in the brecciated zone of the Ruerogai gold deposit (Sichuan province, China; Jambor and Roberts, 2000). In these occurrences this Cu_2Zn mineral is attributed a hydrothermal origin, resulting from wall-rock interaction and reduction by graphite.

Some native lead particles (up to 0.7 mm) have been found in the more reduced clay layers of the coffinite mineralization. Compositions vary from pure Pb to more complex compositions with Cu (up to 5.2 wt %) and As (up to 2.1 wt %; Table 3). The permeability of the Pb-bearing clay of Beverley is low and the recovered grains from the panning concentrates were bright metallic, with some locally bluish area. The grains were clearly preserved from air oxidation in their matrix for the 31 years of core storage.

Zincian native copper is relatively common and is found in a wide range of environments, including lunar regolith, kimberlites, basic and ultrabasic rocks, hydrothermal ores, volcano-sedimentary sequences, and pelagic sediments (Dekov et al., 1999). Native lead in contrast has been documented in a few tens of localities worldwide, but this rarity is likely to be biased because the mineral has frequently been disregarded as a contamination or an artifact. Most of the native lead occurrences are of hydrothermal origin, together with native metals (copper, tin, silver, and gold) or sulfide minerals (e.g., Långban, Sweden; Jonsson and Broman, 2002). Authigenic native lead formed under diagenetic conditions is rare but was observed in the Polish Kupferschiefer (Sawlowicz, 1990), where it occurs in reduction spots in association with covellite, digenite, and pyrite. Modern formation of native lead is mentioned in the well pipes and tanks of the oilfield brines in the Cheleken region in Turkmenistan, where it coprecipitates with sphalerite, galena, and pyrite (Warren, 2000).

TABLE 3. EMPA Analyses of Native Lead Particles

	Pb02	Pb03	Pb04	Pb05a	Pb05b	Pb06
Pb	95.00	91.55	100.26	99.92	90.95	91.20
Cu	<0.19	<0.19	<0.19	<0.19	5.20	<0.19
As	<0.21	<0.21	<0.21	<0.21	2.05	0.61
S	<0.10	<0.10	<0.10	<0.10	<0.10	<0.10
Fe	<0.06	<0.06	<0.06	<0.06	<0.06	<0.06
SiO_2	0.26	<0.20	<0.20	<0.20	<0.20	0.34
K_2O	<0.50	0.81	<0.50	<0.50	<0.50	1.93
P_2O_5	<0.18	<0.18	<0.18	<0.18	<0.18	<0.18
Total	95.26	92.36	100.26	99.92	98.20	94.08

Notes: All values in wt percent; due to the porous texture of some grains, the sums are sometimes lower than 100 percent; undetected: Se <0.16, Co <0.10, Zn <0.21, Ca <0.14, V <0.16, Pd <0.16, Mo <0.19, Ba <0.32 wt percent

The uraniferous nodules

Black nodules of coffinite-uraninite and framboids of carnotite are the only uranium minerals found in the authigenic assemblage. Black uraniferous nodules abound in the mineralized basal silts and sands of the Beverley deposit. Trace amounts of carnotite are present in all nodule-bearing samples, occurring disseminated in the mudstone-clay matrix.

Chemical composition and morphology: The chemical composition of coffinite is variable and its formula was first written as ($U[SiO_4]_{4-x}[OH]_{4x}$) by Stieff et al. (1956). Because of the inhomogeneous nature of coffinite and its water content, the analytical totals of the electron microprobe analyses are frequently under 90 wt percent. Additional analytical problems are due to the fact that the nodules frequently host fine mineral inclusions and are characterized by high porosity. For electron microbeam techniques, the excitation volume at 20-kV accelerating voltage, for a focused beam (1 μm), has a radius varying from ~3.1 to 1.7 μm, depending whether the matrix is porous, silica or uranium rich (Potts, 1987). As a result, the excitation volume in which X-rays are generated systematically contains pores and inclusions of clay minerals or amorphous silica (Förster, 2006). Uraninite commonly forms mixtures with coffinite (Ludwig and Grauch, 1980). Goldhaber (1987) suggested that hydroxyl groups are not present in the coffinite structure; this assumption was confirmed by the infrared (IR) spectroscopic study of Janeczek (1991), which showed the presence of absorbed molecular water but no structural hydroxyl group. Janeczek (1991) proposed the new formula $USiO_4 \cdot nH_2O$. The same author reports a range in (U, Ca, Y, REE)/(Si, P) of 0.93/0.98 *m*, which may reflect intimate mixtures with uraninite.

Several grams of uraniferous nodules were separated from a mudstone sample containing 1 wt percent UO_2 (depth –132 m). The nodules show a black resinous luster on fresh fractures and vary in size from a few tens of micrometers up to 6 mm but are more commonly between 0.4 and 1.0 mm. They frequently contain a Co-rich pyrite core (Fig. 7a, b). The pyrite cores are always spherical and frambroidal. The Co contents of pyrite cores are homogeneous in a single nodule but vary from one nodule to another (Table 4). Small (2-μm) inclusions of clausthalite (PbSe) have been detected by EDS in the compact zones of the coffinite nodules. Microscopically, the coffinite nodules consist of small elongated (oval) particles averaging a diameter of 1 to 2 μm; the smallest coffinite grains from the mudstone matrix share the same bacterioform habit. These bacterioform aggregates are made up by submicrometer-sized crystals (Fig. 7a, b).

The electron microprobe analyses conducted on the nodules are semiquantitative, and the presence of Al is a good indicator of the presence of clay minerals in the excited volume. Coffinite also contains some P (Fig. 8c) and Ca. Sulfur was frequently found in the nodules at concentrations near the detection limit; its presence is certainly related to small inclusions of sulfides in the coffinite matrix (Fig. 7c). The spot

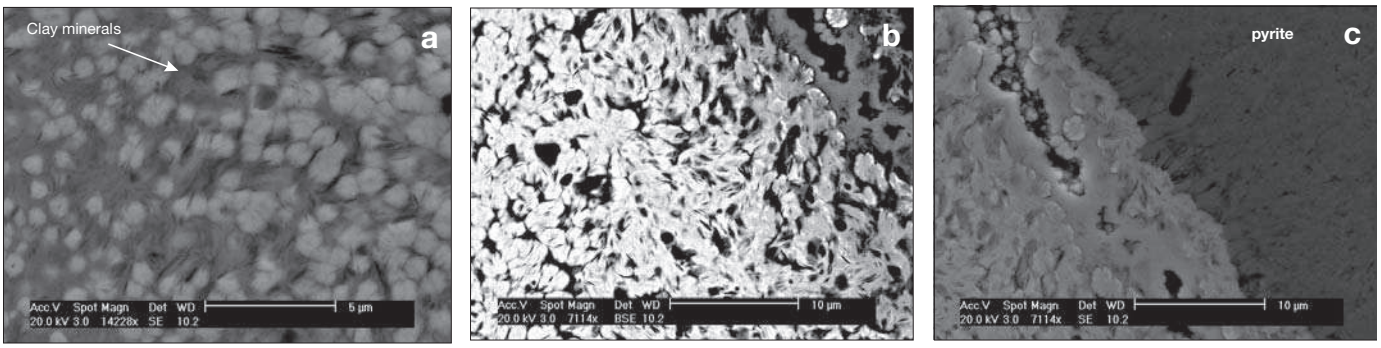

FIG. 7. Coffinite textures revealed by SEM images. Coffinite nodule 157 [–132 m], cobaltian pyrite, and coffinite bacterioform particles. Smectite flakes are also intermixed (black). Photographs (a) and (c) were taken in BSE mode to enlighten the heavy elements (here U). (a) zoom in the outer rim of the coffinite nodule. (b) and (c) a zoom on the pyrite core and coffinite contact.

analyses of the nodule returned between 65 to 92 wt percent UO_2 (Fig. 8b), and single nodules show large variations in chemical composition. The varying U contents are most likely related to the presence of varying amounts of uraninite admixture: a coffinite of stoichiometry $USiO_4 \cdot H_2O$ would contain ~95 percent UO_2 and show a (U + Ca)/(Si + P) ratio of 1.00 (Fig. 8a). Two different mixtures processes are evidenced: coffinite + uraninite and coffinite + SiO_2(am) + water/porosity (Figs. 7, 8a). The admixtures of coffinite and uraninite were confirmed by X-ray powder diffraction performed on 10 mg of nodule material. Rietveld refinement indicates the presence of minor uraninite (25 wt %) and dominant coffinite (75 wt %). The refined unit cell size for uraninite is a = 5.436(1) Å, and for coffinite a = 6.971(2) and c = 6.255(2) Å.

In conclusion, black uraniferous nodules consist of a mixture of coffinite and uraninite, with additional but variable proportions of amorphous silica, detrital quartz inclusions, Co-rich pyrite, clay minerals, and porosity. The fine-grained nature of the coffinite and uraninite crystallites is somewhat problematic for the application of U-Pb dating techniques.

Geochronology and geochemistry: U-Pb dating on coffinite has been successfully applied to some Wyoming sandstone-hosted uranium ores (Ludwig, 1979). However, the coffinite nodules from Beverley are inhomogeneous and porous. Because of this, our LA ICP-MS analyses systematically indicate the presence of high proportions of common lead (often more than 50% of the total lead), whereas the measured isotopic ratios show that the nodules remained more or less open for Pb loss or gain since their formation. Isotopic data corrected for common lead are reported in Table D3. Common lead corrections were applied using ^{208}Pb instead of ^{204}Pb, because of the precision required for the young age expected (<30 Ma) and the relatively low Th/U. Error ellipses are shown in a Concordia diagram in Figure 9, and only three intersect the Concordia curve, giving subconcordant to concordant apparent ages between 6.7 and 0.4 Ma.

Sulfides

Occurrences: Pyrite, marcasite, sphalerite, and chalcopyrite: The two polymorphs of iron disulfide (FeS_2) have been observed: pyrite and marcasite. These minerals are present as individual euhedral crystals, as framboids, or as polycrystalline aggregates. Free pyrite crystals in the Beverley sands can be octahedral, cubic, and cubo-octahedral; pyrite frequently forms clusters of 10 to 30 individuals. Marcasite occurs as single crystals, as twinned fer-de-lance crystals, or as aggregates of parallel individuals aligned on their long axis. Both pyrite and marcasite crystals are up to 400 μm in diameter. Iron disulfides framboids are composite in nature, consisting essentially of pyrite but with a minor component of marcasite. The chemical composition of the free crystals of pyrite and marcasite is always Co poor (<1 wt %), in contrast to that forming the cores of coffinite nodules.

Sphalerite is present in the most reduced level of the coffinite-rich mineralization (Alpha Mudstone), forming framboidal grains up to 2 mm in diameter. Framboids generally host numerous small octahedral pyrite crystals, amorphous silica, and detrital quartz grains.

Minor amounts of very small (<100-μm) chalcopyrite grains have also been observed in the sulfide concentrates. This mineral occurs almost exclusively at a depth of –131 to –133 m in the coffinite-rich layers (Fig. 3).

Sulfur isotopes: Co-rich pyrite cores in coffinite nodules have δ^{34}S values of 1.0 ± 0.3 per mil (bulk analysis on 300 nodules). This contrasts with composite samples of free euhedral crystals of pyrite, marcasite, pyrite, and sphalerite framboids, which give average δ^{34}S values ranging from – 26.2 to –35.5 per mil. Both types of sulfides are authigenic and probably derived from sulfate reduction. The isotopic composition of the groundwater sulfate can be estimated from the isotopic composition of diagenetic gypsum found in soils in the Four Mile Creek catchment: δ^{34}S of 14.0 per mil. This value is similar to those reported for the gypsum in soils and lakes in northern South Australia (Bird et al., 1989; De Caritat and Kirste, 2005).

The prominently negative values found in the free sulfides indicate that they formed at low temperature by bacterial reduction (e.g., Machel et al., 1995); fractionation process due to the reduction of sulfate from waters (e.g., +14‰) will produce sulfides with lighter sulfur composition (–26 ± 10‰). Waters of the Callabonna sub-basin display δ^{34}S values ranging from 11.5 to 17.0 per mil (De Caritat and Kirste, 2005). As a comparison, sulfides from Eocene organic-rich sandstones from the Eyre peninsula and the Eromanga basin sediments (Cretaceous) give negative values between δ^{34}S –6.1 to –18.4 per mil (Bird et al., 1989).

TABLE 4. EMPA Analyses of Co-Rich Pyrite Cores from U-Rich Black Nodules (WC2-73, –132 m)

	1	2	3	4	5	6	7	8	9	10	11	12	13	14	15	16	17	*18*	*19*	*20*	*21*
S	53.55	53.68	51.09	54.17	51.80	53.32	53.39	52.77	52.95	53.53	53.66	52.20	53.65	51.73	52.41	50.05	44.11	45.46	53.32	53.46	54.31
Fe	38.08	45.44	41.62	46.06	46.58	40.88	40.38	39.83	39.50	39.81	47.39	34.32	41.38	35.25	37.54	41.44	39.16	44.25	41.71	44.84	46.04
Co	3.48	0.64	1.39	0.46	0.14	2.13	2.19	2.53	2.62	2.51	0.12	4.68	2.09	4.10	3.13	1.22	1.04	<0.10	1.04	0.32	0.16
As	<0.21	<0.21	0.51	<0.21	0.28	<0.21	<0.21	<0.21	<0.21	<0.21	<0.21	<0.21	<0.21	<0.21	<0.21	0.18	0.41	0.27	<0.21	0.23	0.25
Se	<0.16	<0.16	<0.16	<0.16	<0.16	<0.16	<0.16	<0.16	<0.16	<0.16	<0.16	<0.16	<0.16	<0.16	<0.16	<0.16	0.20	<0.16	<0.16	<0.16	<0.16
Sum	95.11	99.77	94.61	100.69	98.80	96.32	95.96	95.13	95.08	95.85	101.17	91.20	97.12	91.08	93.07	92.89	84.91	89.98	96.07	98.86	100.77

Note: All values are reported in wt percent

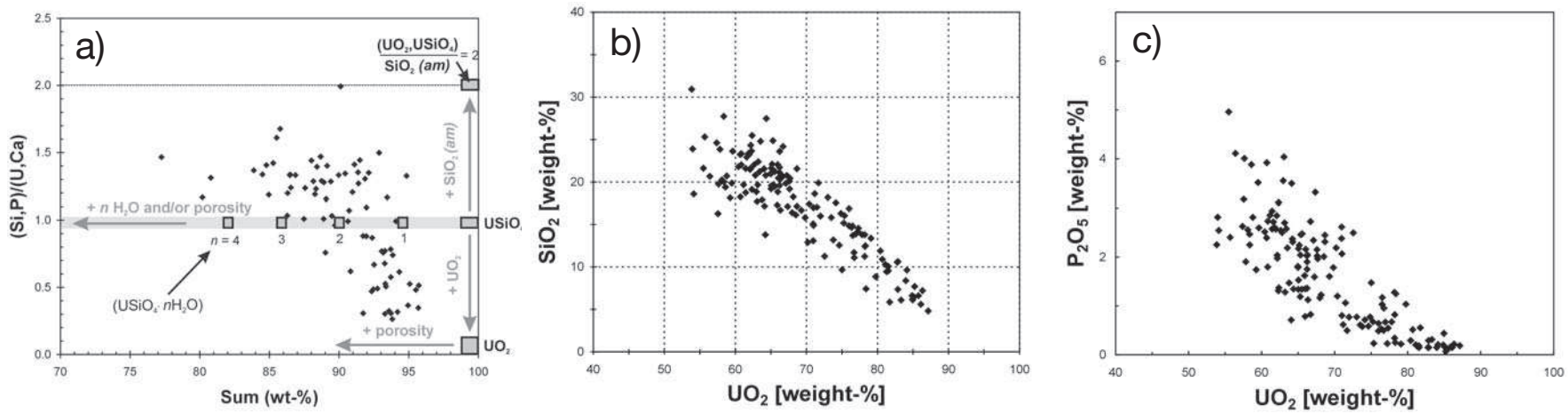

FIG. 8. Chemical composition of coffinite based on EMP analyses. (a). Chemical representation of coffinite nodules by (Si,P)/(U,Ca) ratio and analytical sum. The mixing processes with amorphous silica, porosity, water in the coffinite structure, and uraninite are represented. Dark gray compositions represented are $USiO_4 \cdot nH_2O$, from n = 0 to 4, UO_2 and a mixture of anhydrous coffinite and silica 1/1. (b). SiO_2/UO_2 diagram: compositions fit on a linear trend. (c). P_2O_5/UO_2. Analytical conditions were 1-μm focused beam, 20 nA, and 20 kV.

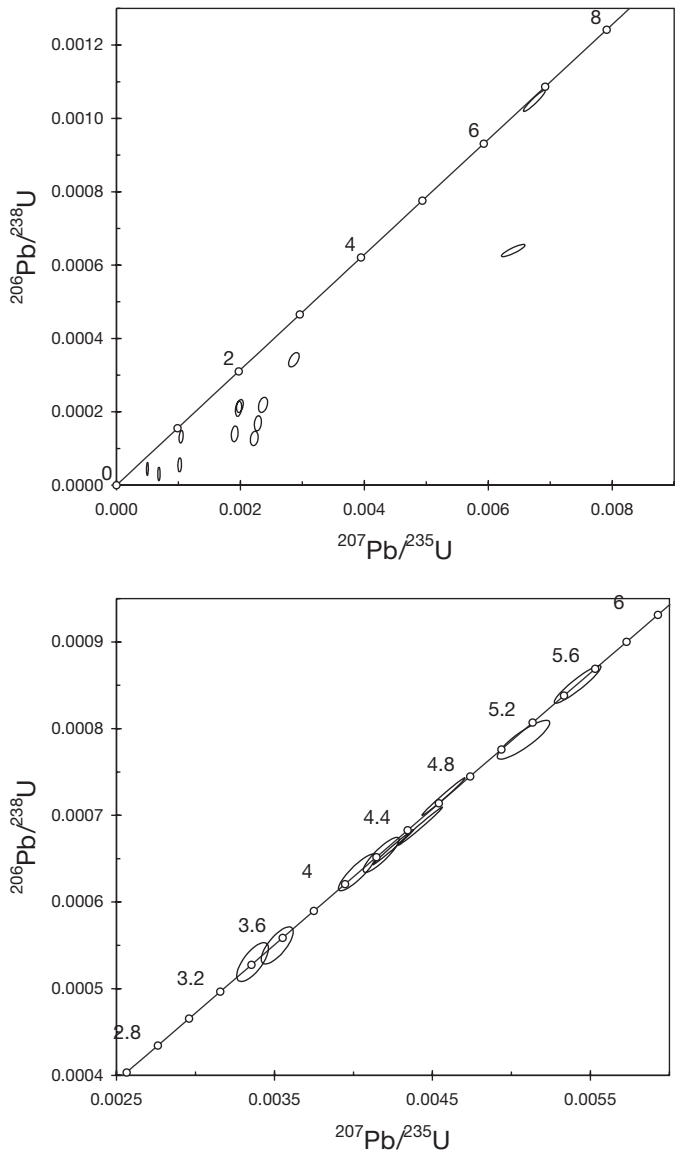

FIG. 9. Concordia plot of (a) coffinite nodules and (b) carnotite. Analyses by LA ICP-MS. No zoning as a function of stratigraphic level could be observed. All analyzed carnotites come from the Beverley Sands and Clays. Coffinite is from the mineralized alpha-mudstone/Beverley Sands contact at level –132 m.

Two explanations can be proposed to explain the isotopic composition of the Co-rich pyrite found in coffinite nodules: (1) Co-rich pyrites were formed by inorganic reduction at temperature >75°C in the presence of hydrocarbons, or a similar reaction involving sulfur from organic compounds (Trudinger et al., 1985); (2) an authigenic freshwater mud-sulfide precipitation (Coleman, 1977; fig. 7.21 in Rollinson, 1993). This later hypothesis is favored, since we there are no indicators of higher temperature fluid circulation.

Sulfates: Gypsum, barite, alunite

Distribution of sulfates: Large diagenetic crystals of gypsum (up to 4 cm) disrupting lamination of Quaternary sandstones are found in the Four Mile Creek alluvial plain. Such gypsum occurrences around the Lake Frome basin have been interpreted to be of evaporitic origin (Draper, 1974). More rarely, gypsum appears as crusts (0.2- to 0.4-mm crystals) on clay fissures of the Namba Formation, where evaporitic conditions have led to the saturation of gypsum in desiccation fissures.

Alunite, $KAl_3(SO_4)_2(OH)_6$, was described by Callen and Tedford (1976) in the WC2 core. The presence of this mineral was confirmed by XRD at depth between –105.8 and –116 m and was also identified via SEM-EDS in the upper layers of the Namba Formation, where it is associated with kaolinite in highly oxidized sediments.

Barite is present in the fine mineralized sediments of the WC2 core as small (<0.5-mm) flat transparent crystals or as spots in the mudstone matrix. Higher concentrations of barite are located in the carnotite zone in association with alunite (Fig. 3). Barite is also found in the coffinite and sulfide zones.

Sulfur isotopes: Gypsum from the Four Mile Creek area has an average $\delta^{34}S$ value of 14.0 per mil. A selection of sulfides (pyrite, chalcopyrite, molybdenite, and arsenopyrite) from the nearby basement rocks was analyzed and found to have a lighter sulfur isotope composition: 1.8 to 10.1 per mil. In the Beverley Sands of the Namba Formation (WC2 core), $\delta^{34}S$ values in barites range between 14.9 and 16.7 per mil (avg 15.7‰). The high values measured in gypsum and barite suggest that the sulfates are the product of crystallization from groundwater (evaporitic conditions) rather than oxidation of sulfides from the basement rocks. However, a mixed origin cannot be excluded. Crystallization of sulfates under evaporitic conditions produces a $\delta^{34}S$ enrichment of around 1.65 ± 0.12 per mil in the crystal phase relative of aqueous sulfate (Thode and Monster, 1965). This is in agreement with the sulfur isotope composition measured farther east in the Callabonna sub-basin and the Yarramba Eocene paleochannel, to the south of Lake Frome (De Caritat and Kirste, 2005). The S isotope composition of the alunite from Beverley could not be analyzed because of its impure and microcrystalline nature. However, alunite from Lake Agar (Eyre peninsula) and Lake Tyrell (NSW) has $\delta^{34}S$ values between 9.0 and 20.0 per mil (Bird et al., 1989), suggesting a sulfur source in the sulfates from waters with minor or no contributions from oxidized diagenetic sulfides (Alpers et al., 1992).

Carnotite occurrence and geochronology

Carnotite, $K_2(UO_2)_2(V_2O_8)\cdot 1–3H_2O$, is part of a mineral group called the uranyl micas, because of their sheetlike crystal structure (Burns, 1999). Potassium ions (K^+) can be replaced by other monovalent ions, such Na^+, Rb^+, Cs^+, Tl^+, and Ag^+. Divalent ions can also be substituted, resulting in the $M(UO_2)_2(V_2O_8)\cdot 3–8H_2O$ structural formula, where M can be Pb, Mn, Ba or Ca (francevillite, fritzscheite, tyuyamunite, metatyuyamunite, and curienite). Owing to the numerous possible substitutions and the interstitial nature of the cations (e.g., K, Pb, and Ba), an important amount of common Pb is expected to be present in natural carnotite. However, the ability of the mineral to retain Pb, or even larger ions like Cs, tends to limit the loss of radiogenic lead from the crystals.

Carnotite is the only U^{6+} and vanadium phase identified at Beverley. It appears as small monocrystals 10 to 20 μm in size

or as frambroidal aggregates up to 1 mm in diameter. It is generally disseminated in the Beverley Sands unit. The mineral has also been observed in cracks within the kaolinite- and alunite-rich samples of the Beverley Clays unit (–100 m) in association with botryoidal allophane. Carnotite forms the upper uranium mineralization, overlying the coffinite-sulfides ore basal level. Its presence at Beverley also explains the high increase in vanadium in the in situ acid-leaching techniques extraction solutions. Electron microprobe analyses reveal that the composition of the Beverley carnotite is close to the theoretical formula $K_2(UO_2)_2(V_2O_8).3H_2O$. The following analyzed elements (given in wt %) were below detection limits (in wt %): Ba <0.28, Pb <0.11, Cs <0.16, Pd <0.18, As <0.22, S <0.06, P <0.10, and Si <0.10. Molybdenum varies between 0.15 and 0.25 wt percent, certainly as minor substitution of VO_4^{3-} as MoO_4^{2-}.

U-Pb isotope data were acquired by LA-ICPMS on carnotite. Because of the total absence of ^{232}Th, a precise ^{208}Pb-based common lead correction could be applied. The calculated ages are all concordant to subconcordant and range from 3.4 to 5.5 Ma (Fig. 9b; results listed in Table D3).

Carbonates

Dolomitic nodules are present in the Namba clays, especially in the Alpha Mudstone, but also in the upper layers capping Namba. This is consistent with the waters of the Miocene paleolake Frome being of hydrogeno-carbonated type, with Ca ≤ Mg and HCO_3 ≥(Ca + Mg) (Callen et al., 1995a; Cojan and Renard, 1997). Dolomite remains a minor phase in the Beverley sediments.

Whole-Rock Geochemistry

The chemical composition of sediments is reported in the deposited Table D4. On average, the sediments from the Willawortina Formation are coarse and contain detritus from the crystalline Mount Painter domain basement. Quartz, K-feldspar, plagioclase, and micas are the dominant components and as a result, the K_2O content is higher than in the Namba Formation. High levels of Y, REE, Th, Nb, and Ta reflect the presence of material from the Mesoproterozoic granites that is dominant in the Willawortina Formation. The kaolinite-rich levels of the upper Namba Formation display high sulfate concentrations related to alunite, gypsum, and barite.

Trace elements and geochemistry of the mineralization

Trace elements patterns reflect mainly the chemistry and mineralogy of the host sediments but also the geochemical overprint of the uranium mineralization. As the detailed ore mineralogy has now been identified, we can assign some trace and minor elements to specific minerals. Carnotite mineralization is observed in the sulfate zone of the upper strata of the Namba Formation. Uranium concentrations vary from 7 to 50 ppm and V from 65 to 125 ppm in these rocks. Sulfate-rich layers (alunite and gypsum) show elevated Sr and less marked increases in Ba, Pb, Cu, and Mo (the later associated with carnotite). The sulfate layers are highly oxidized with a measured whole-rock Fe^{2+}/Fe^{3+} ratio less than 0.05.

The finer sediments of the Namba Formation below the Beverley Sands (clay, silts, and fine sands of the Alpha Mudstone) are more reduced and also contain the coffinite-uraninite and sulfide mineralization. Uranium reaches 1.0 wt percent UO_2 in the richest sample analyzed. The following elements show a positive anomaly related to the coffinite nodules: Ni, Co, Cu, Zn, Pb, V, As, Mo, and REE. The coffinite-rich sample from this Alpha Mudstone interval at the contact to the Beverley Sands is relatively reduced (Fe^{2+}/Fe^{3+} = 0.31), and the samples of Alpha Mudstone (–132 to –135 m level) contain visible amounts of organic matter.

Samples 968 and 969 (Beverley Clays, –106 to –111 m) contain alunite intermixed with kaolinite and have elevated Sr (>1,000 ppm), low Ca/Sr ratios (<5.0), together with 0.14 to 0.23 wt percent P_2O_5. Alunite group minerals can accommodate large cations in the A site (Ca, Sr, and Ba) replacing K. At the same time, PO_4^{3-} can partly substitute SO_4^{2-} (Stoffregen and Alpers, 1987; Li et al., 1992). We attribute these patterns to the alunite group minerals. The samples also have very low Fe^{2+}/Fe^{3+} ratios.

REE patterns

In general, samples from the Willawortina Formation have much higher REE concentrations than those from the Namba Formation, reflecting the contribution of the Mesoproterozoic granites (Fig. 10a). Post-Archean Australian Shales (PAAS) REE patterns in the bulk coffinite mineralization show a bell shape centered on intermediate REE (Sm-Dy). This is further confirmed by measurements in coffinite that display REE concentrations centered on Tb (Fig. 10b). REE in the coffinite mineralization are strongly fractionated with La_N/Sm_N = 8.

The underlying Alpha Mudstone adjacent to the mineralization shows enrichment in HREE (Ho-Lu), which probably records the path of an REE-rich fluid depleted in intermediate REE and some adsorption process in the clay minerals (Fig. 10a). This HREE enrichment is not related to coffinite (U <<REE) or detrital heavy minerals.

The carnotite-rich layer with kaolinite and alunite possesses the lowest sum of REE (80 ppm). Although uranium is present in carnotite, REE are not concentrated in the rock and the REE patterns indicate that the REE contents of the carnotite-rich layers are controlled by the detrital minerals monazite-(Ce) and zircon.

Interpretation of Data

The multiple datasets, analyses and observations produced during this study are discussed in several categories: paleoenvironment and origin of the sediments, age of the mineralization, physicochemical conditions of deposition, and possible sources of uranium.

Paleoenvironment and origin of the Beverley sediments

Alpha Mudstone: The Alpha Mudstone unit, which hosts the lower level of the Beverley mineralization, is clay rich (smectites) and poor in heavy minerals that are released from the local Mount Painter domain basement. The sediment is characteristic of low-energy lacustrine environment and contains organic material. High Fe, Mg, and Al contents reflect the clay content and the presence of palygorskite or dolomite records the Mg-Ca-hydrogeno-carbonated water chemistry for the Miocene Lake Frome (Callen et al., 1995a; Cojan and Renard, 1997). The clays also contain zircon fragments with

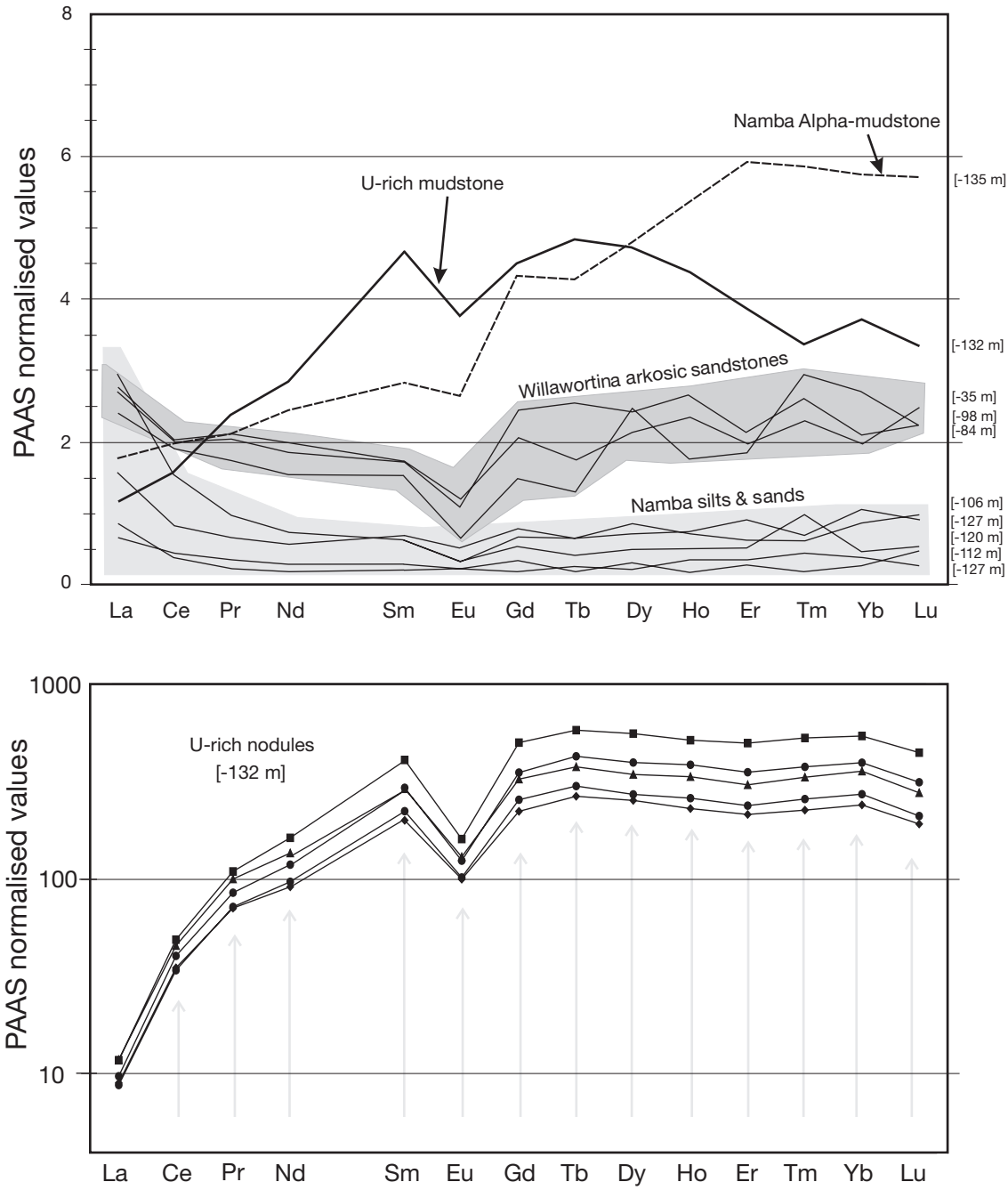

FIG. 10. Post-Archean Australian Shales (PAAS)-normalized (McLennan, 1989) REE spectra for Beverley sediments and coffinite nodules. (a). The three units present different patterns and only overlap around the light REE area. Willawortina sediments display much higher REE concentrations related to the high proportion of material sourced in the local Mesoproterozoic granites. The mineralized mudstone is showing a very high intermediate REE curve. The Alpha Mudstone which immediately underlies the uranium mineralization is also showing very high intermediate REE values and the highest heavy REE values; it probably indicates the presence of a Y-rich phase (e.g., xenotime). Layers –106 and –111 contain the alunite-jarosite minerals; it coincides with the lowest REE values (depletion). (b). The coffinite nodules show a strongly enriched intermediate to heavy REE signature that correlates with the whole-rock composition.

volcaniclastic morphology (Fig. 11). The proportion of Mount Painter domain-related zircons in the Alpha Mudstone (D typology) is low, and rutile is clearly dominant over zircon (Fig. 4, Table D1). Hence we interpret the Alpha Mudstone to be mainly sourced from outside the Mount Painter domain, from a source region rich in S- or I-type granites (based on zircon typology) and associated metamorphic rocks (high proportion of rutile) with a significant volcanic or volcaniclastic materials contribution (zircons morphology).

Beverley Sands: The next unit, the Beverley Sands, is coarser than the Alpha Mudstone, consisting of kaolinite-bearing silts and fine sands. Kaolinite is thought to be sourced

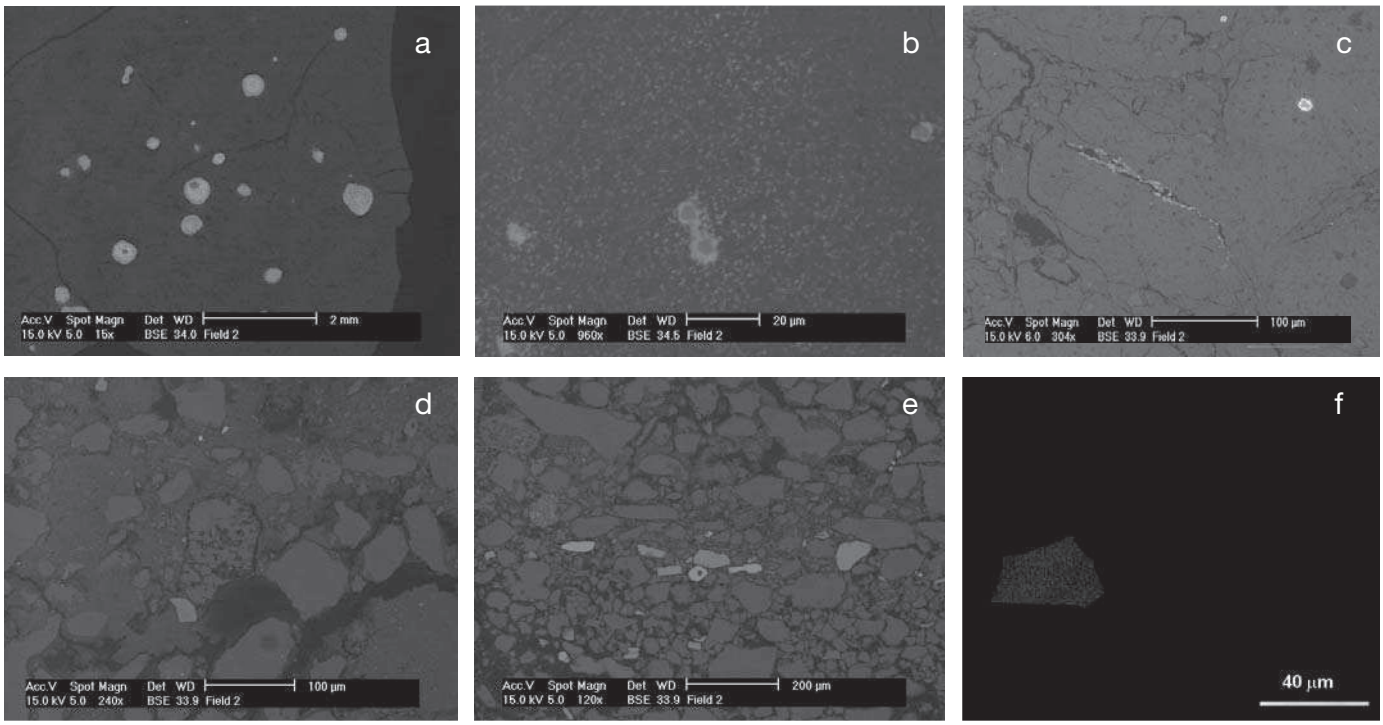

FIG. 11. Disseminated coffinite and heavy minerals from the Beverley sediments. (a). Coffinite nodules in mudstone-claystone matrix. Some display pyrite cores (–132 m). (b). Extremely small (2 μm) disseminated coffinite in mudstone (–132 m). (c). Coffinite nodule (white) and organic matter in mudstone (black). A pyrite layer underlines organic matter (–134 m). (d). Fragment of zircon (light) next to a weathered euhedral crystal of albite. (e). Heavy mineral bedding in very angular quartzose sandstone. Zircons (white) and ilmenite (light gray). (f). Extremely fragmented fresh zircon of interpreted ignimbritic origin in a mudstone matrix.

from the weathering of the local kaolinized regolith and, possibly, from outcropping granite saprolite. The dominant mineral is quartz; its morphology is very angular, excluding long distance alluvial transportation (Fig. 11). However, the feldspar proportion is very low and this excludes a proximal fluviatile deltaic origin from the Mount Painter domain basement. The heavy mineral assemblages are poor in Fe-Ti oxides, in contrast with the Alpha Mudstone and the MPD, the later containing a high proportion of hematite and magnetite.

The combination of selective geochronological and typologic approaches used for the study of the zircon population of the Beverley Sands provides considerable information about their origin. Age populations show a dominant Permo-Carboniferous grouping, a Devono-Ordovician grouping, and a Jurassic-Cretaceous–aged group (Fig. 6). The only possible source for the Early Cretaceous to Jurassic zircons lies in the eastern Australian volcanic province (Whitsunday volcanic province), a calc-alkaline volcanic arc extending along the eastern margin of the former Gondwana (Bryan et al., 2000). This province is also referred to as the Tasman arc (Sircombe, 1999), and the only other region that could have supplied similar material of this age is in Antarctica (Fig. 12). The major Permo-Carboniferous zircon population probably originates in Eastern Australia in the New England fold belt. The remaining population of Devonian to Ordovician zircons can also be originated in the Lachlan fold belt orogen granitoids, which extend from northern Queensland to southern Victoria. As mentioned by Sircombe (1999), zircons of Cretaceous-Jurassic age are present in the Eromanga and Surat basins (Fig. 12). The Cretaceous volcanics and granitic rocks are presently located in the eastward watershed of the Great Dividing Ranges, indicating a major change in paleorelief and drainage directions since the Miocene.

The lack of rounding and mechanical wearing on the crystal surfaces of Mesozoic to Paleozoic zircons is consistent with the angular quartz grains in the formation. We envisage two possible transportation processes for this material: (1) aerial volcanic dispersion during major ignimbritic eruptions, which may extend for up to 150 km, however, the eastern Australian volcanic province is over 1,400 km away; (2) glacial dispersion during the Early Cretaceous (144–131 Ma) glaciation documented by Alley et al. (2003). Though volcaniclastic dispersion has probably contributed to the dispersion of Cretaceous zircons, it is unlikely to explain the broad assemblage of Paleozoic to Mesozoic ages in the Beverley Sands, and it cannot explain the angular morphology of the host sands. In contrast, the age of the glaciation coincides with our youngest dated zircons (130 ± 3 Ma), and glacial transport hence can explain the absence of younger Cretaceous zircons present in the Eastern Australian volcanic province (up to 95 Ma). Cretaceous glacial transport can also explain the presence of both fresh Permian-Carboniferous zircons and angular quartz-rich sands. We therefore consider the glacial transportation as the most plausible process for bringing the Beverley Sands source

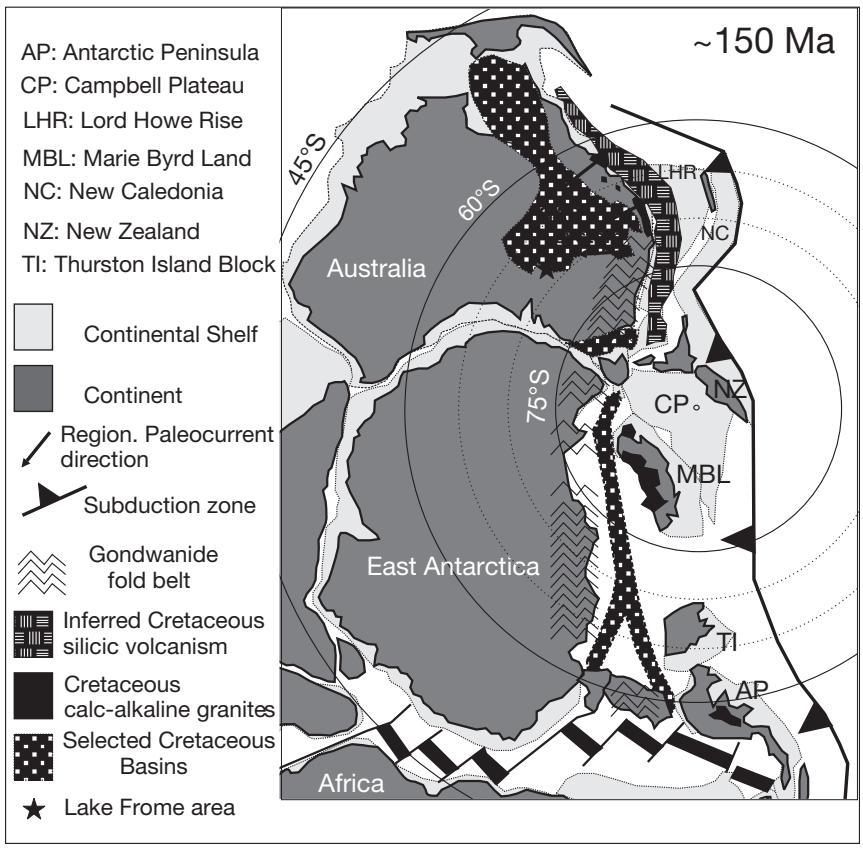

FIG. 12. Polar projection of the southern Gondwana area at ~150 Ma. The relative position of Australia and East Antarctica remains identical until 80 Ma. Subduction under the eastern margin of Australia and/or East Antarctica is accompanied by silicic explosive volcanism and calc-alkaline magmatism. The volcanic arc and the eastern Australian mountains range are both drained into the inland basin (Eromanga basin or GAB). Paleolatitude and relief also allow extensive glaciers spreading (modified from McLoughlin, 2001).

material into the Lake Frome basin. The area between Brisbane and Townsville (Queensland) where Cretaceous granites and volcanic rocks abound (Fig. 12) is the best potential source area. Paleogeographical reconstitutions give a ~70°S paleolatitude for this location at 150 Ma, which consisted of mountain chains of over 1,000-m altitude at the time (Veevers, 2006). This setting is ideal for sourcing glaciers, and it is likely that the path of such glaciers extended over the Eromanga basin toward the southwest.

The Beverley Sands hence contain mainly reworked Early Cretaceous glacial and fluvioglacial and/or glacio-lacustrine materials. The fine granulometry of the formation and the presence of kaolinite can be explained by low energy washout of these Cretaceous materials in a lacustrine environment. The mineralogical maturity of the assemblage (quartz-rich sand with advanced Fe-Ti oxide disappearance) can be explained by the intense weathering of the Cretaceous formations during the Miocene-Oligocene period. The paleoenvironment of deposition of the Beverley Sands unit is therefore interpreted as a Miocene shoreline of a freshwater lake, along which Cretaceous sediments washouts were redeposited.

Beverley Clays: The mineralogy of the Beverley Clays unit is dominated by kaolinite and quartz with locally abundant alunite. The source of the sediment is interpreted to be similar to the Beverley Sands unit, with the mineralogical differences reflecting a change in depositional environment. The nonmagnetic heavy minerals reveal an abrupt change in relative proportions between the Beverley Clays and the Beverley sands. The rutile index [$Ru/(Ru + Zr)$] increases from 0.1 to 0.7 in the Beverley Sands to 6 to 50 in the Beverley Clays; this could be related to a sedimentary change but also be the result of a selective mineral disappearance during weathering. Due to the overall immaturity of the sediment, a change in sedimentary source remains the most likely explanation. The distribution of corundum also provides additional evidence for a change in the sedimentary source. Corundum is quite rare in the Beverley Sands and suddenly becomes abundant in the Beverley Clays above the −106-m level. Occurrences of corundum are widespread in the Mount Painter domain, especially in the Radium Creek Metamorphics and the Freeling Heights Quartzite in the Mount Adams area. This suggests that the Mount Painter domain starts to be a more important source of detrital material during the deposition of the Beverley Clays, and this could relate to an episode of exhumation. The appearance of corundum also coincides with kaolinite in the upper part of Namba and records a change from lacustrine to emerged conditions. Sulfides were oxidized leading to the development of acidic soils and to the formation of alunite.

Willawortina Formation: The heavy mineral assemblages in the Willawortina Formation show a wide variety with numerous U-REE-Th-Y minerals reflecting the major component sourced from the Mesoproterozoic-Paleozoic basement rocks of the Mount Painter domain. The zircon typology also indicates a dominant Mesoproterozoic granite-gneissic origin. The sedimentary sequence of the Willawortina Formation coincides with the last period of intense uplifting in the North Flinders Ranges.

Timing of the mineralization

The uranium mineralization at Beverley is hosted in the Miocene to Pliocene Namba Formation. Palynology data constrain sedimentation between ~24 and ~6 to 4 Ma (Martin, 1990), whereas zircon population ages identified do not constrain these limits (youngest measured zircon is 130 Ma). Concordant U-Pb ages obtained on carnotite suggest a late Miocene to early Pliocene mineralizing event, between 5.6 to 3.4 Ma. Some coffinite mineralization may have formed earlier, based on a single concordant age at 6.7 Ma. Unfortunately most U-Pb data on coffinite are discordant, indicating some open-system behavior. These data however clearly indicate that the mineralizing event occurred prior to the major Pliocene uplift, which led to the buildup of the thick Willawortina Formation (3.5–0.7 Ma).

Physicochemical conditions during mineralization

The local environment during the Miocene was lacustrine and changed to arid conditions during the Pliocene, with emergent conditions and soil development. Several syndiagenetic processes can be envisaged that could drive U mineralization during this changing paleoenvironment: (1) a direct adsorption and reduction of uranium from oxidized groundwaters into the organic matter-bearing lacustrine mudstones (Upper Alpha Mudstone) and quartz-rich sands on the lake shores (Beverley Sands). Note that no organic matter is preserved in the Beverley Sands, suggesting either total oxidation of organic matter in this porous unit, or reduction by migrating hydrocarbons, or reduction by microbiota; (2) a later paleosoil forming in an emerged environment with arid conditions; intense weathering of the outcropping outwash plain sediments and basement; and (3) mixing of reduced basement brines with shallow oxidized groundwaters along the syngenetic Poontana fault structure.

Chemistry of groundwaters: The nature of the waters prevailing during the deposition of the Namba lacustrine sediments is constrained by the presence of dolomitic nodules. These are present in the Namba clays, especially in the Alpha Mudstone, but also in the upper layers capping the Namba Formation. The combined presence of dolomite and palygorskite in the sediments implies that the waters of the paleolake were of hydrogeno-carbonated type, with Ca ≤ Mg and HCO_3 ≥ (Ca + Mg). The transportation of uranium in this type of waters is controlled by uranyl carbonate complexes such as $[UO_2(CO_3)_3]^{4-}$ (e.g., Brugger et al., 2005). No direct evidence is available to support the possibility that part of the high U nodules in the Alpha Mudstone are of syngenetic origin. The paleoenvironment then changed from lacustrine to littoral conditions (Beverley Sands) and finally to emergent conditions. The present groundwater composition at Beverley and in the neighboring bores is available from the literature: the Namba aquifer (Beverley Sands) bears $1.6 \cdot 10^{-2}$ *m* $[SO_4^{2-}]$, $5.6 \cdot 10^{-2}$ *m* $[Cl^-]$, and ~$4 \cdot 10^{-3}$ *m* $[HCO_3^-]$; $[HCO_3]$ << [Ca + Mg] and [Ca] ≈ [Mg] (Ker, 1966; Heathgate Resources Pty. Ltd., 1998). The measured pH is 7.6 and the temperature in the Beverley Sands aquifer is around 25°C. These data have been used for the building of the $\log f_{O_2}$-*p*H diagrams shown in Figure 13. Calculations of saturation indices (SI; Bethke, 1996) for Beverley water show that barite and gypsum have SI between –1 and 1, suggesting they still control the present groundwater chemistry.

Reduced mineralization: The reduced uranium mineralization at Beverley is characterized by coffinite (±uraninite) and pyrite. These three minerals represent >90 percent of the authigenic minerals. Smaller amounts of sphalerite, native copper, chalcopyrite, and barite are also present. Carnotite is present in small quantity relative to coffinite (<1%), and chalcopyrite, native lead, and a copper-zinc alloy are extremely rare accessories. The presence of native lead in the reduced ore zone provides strong constraints on the physicochemical conditions as this mineral forms in environments where the activity of reduced sulfur species is extremely low (Fig. 13d); Sawlowicz (1990) suggests that native lead forms in microenvironments where decomposing organic matter is able to liberate organic bases or NH_3 into solution ($f_{CH_{4(g)}} >> f_{CO_{2(g)}}$). These conditions are met in the mudstone, which contains organic matter clasts surrounded by an impermeable matrix. Native lead hence documents the extreme reducing conditions that prevailed locally during ore genesis.

The presence of native Zn in the native copper particles does not require stronger reducing conditions than formation of pure Cu. Native Zn itself is not stable in the presence of water. Physicochemical changes are also observed on the rims of native copper particles, which often display a cuprite (Cu_2O) and minor tenorite and/or malachite rim. The presence of sphalerite and minor chalcopyrite within parts of the coffinite mineralization can be explained by stronger reducing conditions, independent of sulfur concentration (Fig. 13b). The role of microorganisms in the development of these reduced microenvironments is supported by the strongly negative $\delta^{34}S$ values in authigenic sulfides (sphalerite, Co-poor pyrite, marcasite), hinting to bacterial reduction of sulfates from groundwater. Positive $\delta^{34}S$ in Co-rich pyrite cores in coffinite nodules is interpreted to result from an early freshwater mud-sulfide precipitation in the lacustrine environment and predates the uranium mineralization. Goldhaber et al. (1987) described the formation of coffinite as a combined adsorption and reduction process. They found that high dissolved silica concentration favors coffinite versus uraninite, as predicted from thermodynamic considerations (Fig. 13c; see also Brugger et al., 2005). Goldhaber et al. (1987) also showed experimentally that uranyl adsorbed on kaolinite surfaces is quantitatively reduced by dissolved H_2S (pH = 7, 35°C, p_{H_2S} = 0.081 atm). Part of the coffinite nodules mineralization may have occurred by reduction of the UO_2^{2+} by dissolved H_2S during an early stage of mineralization, though it is not possible to clearly assess this hypothesis at this stage. It is important to note that the coffinite nodules present the criteria listed by Cai et al. (2007) in favor of an origin via bacterial reduction: association with fine-grained sulfides and with

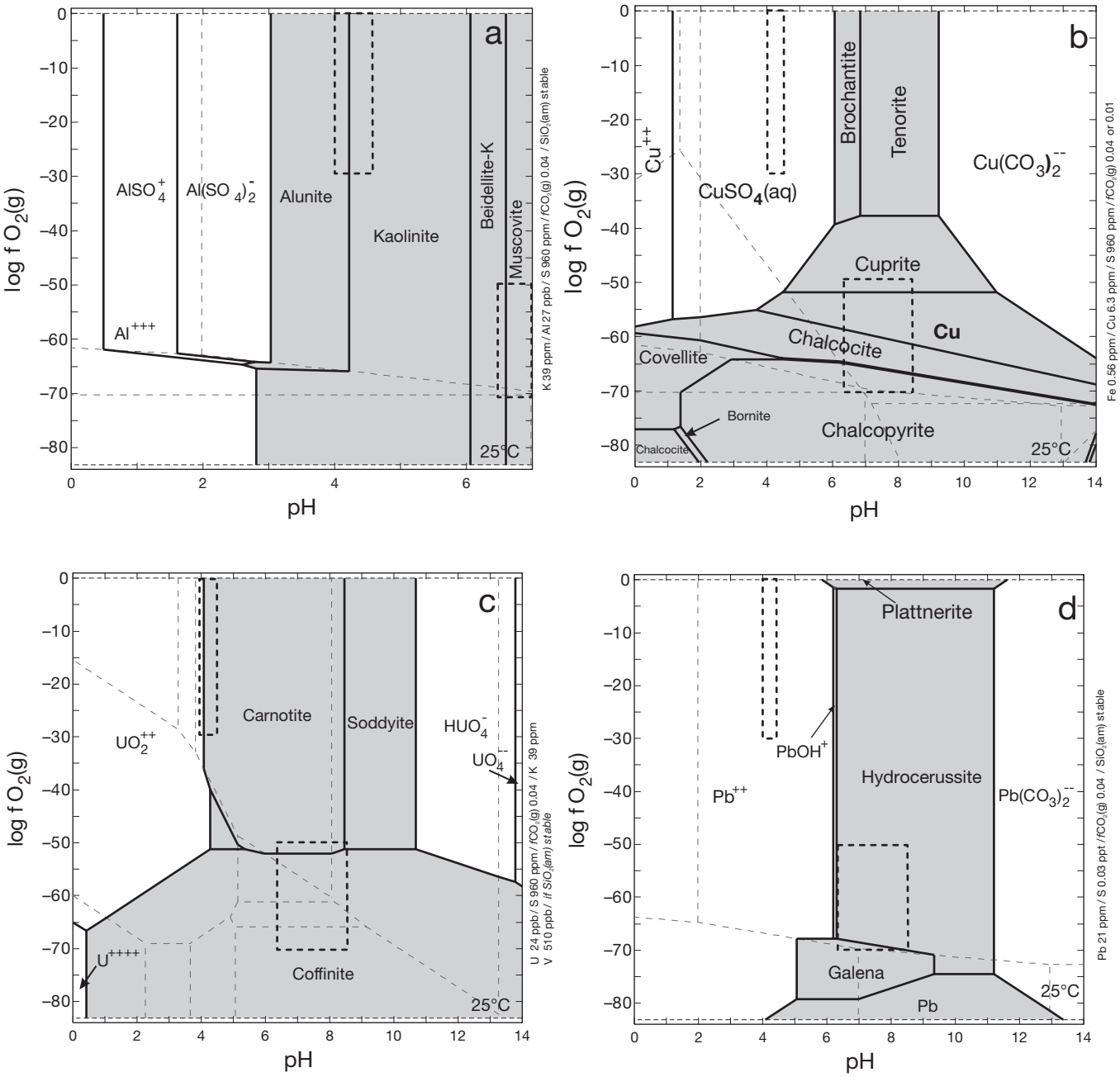

FIG. 13. Log $f_{O_2(g)}$ vs. pH diagrams for U, Cu, Pb, Zn, Fe, and Al. The diagrams are based on the water compositions measured in the Namba aquifer around the Beverley mineralization. Two different S concentrations are shown in (d) (960 ppm and 0.03 ppt S). Two fields are drawn to represent the conditions to form mineral assemblages observed in the mineralizations: oxidized and /or reduced mineralization. All calculations were done using the Geochemist's Workbench (v. 6; Bethke 1996), with thermodynamic data taken from the Lawrence Livermore database (LLNL. V8R6).

phosphorus and potassium; bacteriomorph morphology (Fig. 8) with individual crystals having nanometer sizes. This suggests that bacterial reduction may have been a predominant process at Beverley, especially in the Beverley Sands that apparently lack organic matter.

Oxidized mineralization and alteration: Carnotite at Beverley is widespread in the silts and sands and is also commonly associated with coffinite. Carnotite is very stable in relatively oxidized groundwaters and requires very little vanadium to form (Fig. 13c). This means that vanadium cannot be carried simultaneously with uranium, and carnotite precipitation is likely to occur in V-rich microenvironments, such as V-rich clays or accessory V-rich minerals, or via mixing of V-rich groundwaters with U-rich ones. The samples containing the highest concentrations of carnotite occur at the top of the mineralization (Beverley Clays) and are also kaolinite-rich and alunite-bearing sections. In addition to these minerals, we observed some hematite or goethite bands, which suggest

local oxidation and remobilization of Fe sulfides. This is confirmed by the absence of Fe^{2+} in whole-rock analysis.

Alunite forms under acidic conditions (pH <4.5) and its presence together with kaolinite and carnotite restricts the forming conditions of the mineral assemblage (Fig. 13a, c). The prevailing conditions are estimated to be between pH 3.9 to 4.5, with $\log f_{O_2}$ from atmospheric to −30 (oxidizing conditions). Based on the presence of a paleosoil with roots remnants at the −100- to −102-m levels in the WC2 core and on the absence of sulfides from −100 to −116 m (Fig. 3), the alunite of Beverley is likely to have formed in a lacustrine-marsh system by surficial sulfide oxidation. Alunite has been found in modern acid lakes from eastern Australia (Bird et al., 1989; Long et al., 1992). Mobilization of uranium during surface oxidation of sulfidic sediments was proposed by Weeks et al. (1959) to explain the Colorado carnotite ore, with oxidation of exposed pyrite-rich coffinite ores leading to acidic conditions, uranium redissolution, and finally carnotite precipitation.

REE geochemistry: The Willawortina Formation has high REE contents of ~400 ppm, reflecting the predominant source of sediments within the Mount Painter domain granitoids. The mineralized silts at the base of the Beverley Sands (−132 m) show a distinctive enrichment in medium REE, while the coffinite-uraninite nodules show a general enrichment in HREE with a distinct preference for intermediate REE centered around Tb (Fig. 10). HREE fractionation is a common feature of coffinite and/or uraninite (Hansley and Fitzpatrick, 1989; Janeczek, 1991). The underlying Alpha Mudstone displays a strong enrichment in HREE just below the uranium mineralization, which can be explained as the result of interaction between clay minerals and HREE-rich mineralizing fluids. Nesbitt (1979) observed preferential HREE mobility during the weathering of a granodiorite in east central Victoria (Australia), leading initially to an enrichment of HREE in the weakly weathered rock, to a strong depleting in HREE in the deeply weathered rock. Experiments on REE mobility during alunite-jarosite dissolution under acidic conditions at pH 3 and 4 have shown that intermediate REE are preferably leached from the sediments (Welch et al., 2007); hence intermediate REE enrichment could possibly be linked to Pliocene acid soil formation. However, given the complexity of mineral-fluid interaction (e.g., Brugger et al., 2008), other mechanisms may explain this REE signature. The high REE contents of the mineralization, however, can clearly be linked to the REE-rich basement of the Mount Painter domain.

Source(s) of uranium

Where does the uranium source lie? In the words of R. W. Haynes (1975, p. 813), "The geomorphology of the area and the proximity of the Beverley sedimentary uranium deposit to the relatively rich uranium source rocks of the Mt. Painter complex provide such an obvious association that it would be difficult to seriously consider any alternative origin for the uranium contained in Beverley." The same author also comments on the dispersion of radioactive minerals from the uranium-rich basement rocks into the Lake Frome embayment visible in airborne-radiometric exploration maps. Brugger et al. (2005) showed that reduction of the modern groundwaters located within U-rich Mount Painter domain granitoids would result in Beverley-type ores. However, the current drainage, topography, and hydrochemistry do not necessarily reflect the paleoenvironment during which mineralization formed. For this reason, we review the available regional uranium reservoirs and discuss their potential as a source for the uranium at the Beverley deposit (Table 5).

The presence of intermediate REE-enriched patterns in the uranium mineralization strongly favors an origin in REE-bearing rocks or sediments. More precisely, the REE in the ore can originate from accessory minerals, such as polycrase-(Y), euxenite-(Y), monazite-(Ce), or allanite-(Ce), which are very common in the Mount Painter domain basement and related Willawortina Formation. These minerals are however rare in sediments of the Namba Formation. The presence of a minor population of Mesoproterozoic zircons in the Beverley Sands indicates that the Mount Painter domain was perhaps subcropping during the Miocene, and this provides an argument in favor of the direct derivation of uranium from the Mount Painter domain as early as during the Miocene.

The acidic conditions (i.e., pH <4.5) recognized in the Beverley Clays can efficiently leach uranium from heavy minerals, such as zircons, allanite, thorite, monazite-(Ce), polycrase, etc. Massive amounts of U and other traces can be liberated under acidic oxidizing conditions (Bajo et al., 1983a, b). From the average composition, zircon contributes ~10 percent of the total U and 1.5 percent of the total REE in the Willawortina and Namba sediments. In the proximal Four Mile Creek sediments, the dominant hosts for U and Th are xenotime and monazite-(Ce) (~60% of total U). Highly unstable U rich minerals like samarskite or polycrase and brannerite are also present in these sediments and contribute to at least a few percent of the bulk U. In conclusion, it is important to point out that both the Willawortina Formation and the Mount Painter domain basement rocks have a much higher availability of U for leaching than the Namba sediments.

The potential of these identified sources is shown in Table 5 together with an estimation of the available quantities of uranium. This was calculated using the different reservoirs size, average U concentrations, and estimating its availability coefficient to release based on the average mineralogy: 1.0 for total availability to leaching (e.g., coffinite, uraninite), 0.2 to 0.1 for Mount Painter domain basement rocks or Willawortina sediments (high metamict heavy minerals content), and down to 0.05 in the case of uranium in the Namba sediments (U in crystalline heavy minerals mostly; Table 6).

Considering the tonnage of the Beverley mineralization, including the sub-economic and unrecoverable resources, a global estimation of the contained uranium in mineralization sits around 30,000 t U_3O_8. The scale of the mineralization requires other sources than the Namba aquifers (~1,000 t U_3O_8) or its weathered alunite-kaolinite capping (~300 t U_3O_8). In addition, because of their downstream location, these two reservoirs are not suitable for the genesis of the Four Mile deposit. The basement of the Paralana High Plains, which is outcropping in the vicinity of the Paralana Hot Springs, is also considered too small to have provided enough uranium for Beverley. The availability of this reservoir to uranium liberation is also subject to interpretation in the absence of an exact knowledge of its uranium content and whether it had some connection to the Namba aquifers.

TABLE 5. Uranium Reservoirs and Their Possible Link to the Beverley Uranium Deposit Genesis

Uranium reservoir	Arguments for	Arguments against	Missing information
Namba Formation (sandy aquifers)	Presence of acid volcanic material (rhyolites, dacites) in the sediment	Contains organic matter (U trapped) Low U content compared to other reservoirs (<10 ppm U) The Beverley Sands are of limited extend and represent a littoral lacustrine formation	
Namba Formation (kaolinite-alunite layers)	Leached under acidic and oxidative conditions Presence of secondary U minerals Higher % of heavy mineral from Mount Painter domain basement (corundum, U-rich zircons) *m*REE-enriched signature of the coffinite ore	Kaolinite and alunite layers derive from the reworking from clayey pyrite-rich material More likely to be a residual formation of mineralized Alpha Mudstone and/or Four Mile ore type Carnotite ages fit in the range 5.3 to 3.1 Ma, which is identical to the layer attributed age (pre-3.5 Ma)	Dating of alunite by K-Ar or Ar-Ar technique Sulfur isotope on alunite
Willawortina Formation	High U, REE, and Th content (40 ppm U) with high proportion of metamict minerals	Willawortina Formation mostly postdates the dated mineralizing event (5.3 – 3.1 Ma) Willawortina and Namba aquifers are not connected	
Paralana High Plains crystalline basement	Presence of kaolinite in several levels of Beverley (feldspar alteration directed from basement rocks) High U content Proximity (present-day upstream) Location next to Poontana fault that may have be a conduit for fluids	Was essentially not outcropping and is partly capped by Cretaceous formation Modern-day deep groundwaters such as Paralana High S is reduced (H_2S stable) and U poor	Lack of knowledge on the basement nature (granites, rhyolites, metasediments)
Four Mile uranium deposit	Proximity (upstream) Uplift of the Paralana High Plains may have provided exposition of the ore to surface, developed acid sulphate soil	Four Mile deposit could postdate the Beverley deposit Similar grades of uranium could suggest similar genesis but not remobilization downstream from Four Mile	No information on possible weathered top soils horizons No geochronology data No geochemical or mineralogical information
Crystalline basement of the Mount Painter domain	Presence of the Four Mile deposit even closer to the Mount Painter domain High U in the watershed (frequently >100 ppm U) Was sub- or outcropping before 3.5 Ma; presence of Mesoproterozoic zircons (favors chemical over mechanical U transportation) Presence of angular sands in the Beverley Sands with Cretaceous zircons; this indicates low-energy transportation from Cretaceous formations Major Miocene uplift on Paralana fault (dated by fission tracks)	Was possibly covered by Cretaceous sediments (<5 ppm U) over large parts	Lack of information on the orientation of the watershed over the Mount Painter domain during Pliocene and Miocene

TABLE 6. Mass-Balance Calculation and Evaluation of the Potential Uranium Reservoirs for Beverley

Uranium reservoir	Evaluated size	Volume (km^3)	U (ppm)	U availability coefficient	Reservoir ($\times 10^6$ ton)	U reservoir (t U_3O_8)
Namba Formation (sandy aquifers)	15×5 km^2 $\times$ 20 m	1.50	7	0.05	2,700	1,113
Namba Formation (kaolinite-alunite layers)	15×0.4 km^2 $\times$ 2 m	0.012	15	0.80	21.6	305
Willawortina Formation (1)	12×6 km^2 $\times$ 50 m	3.60	35	0.15	7,920	48,993
Willawortina Formation (2)	6×2 km^2 $\times$ 50 m	(0.60)			(1,320)	(8,165)
Paralana High Plains crystalline basement	5×5 km^2 on 10 m (saprolith)	0.25	30	0.10	550	1944
Four Mile Uranium deposit type	1×0.3 km^2 $\times$ 2.5 m	0.0008	5,000	1.00	1.65	9721
Crystalline basement of the Mount Painter domain	25×8 km^2 $\times$ 10 m (saprolith)	10	25	0.10	22,000	64,805

Although the Four Mile deposit has not formally been included in this study, it is necessary to include it in the discussion and to consider the same reservoirs for its genesis. The deposit has a combined indicated and inferred resource of 31,505 t U_3O_8 at an average grade of 0.3248 percent (Alliance Resources Pty. Ltd., 27/01/2010 press release). The Four Mile deposit is hosted in sands of the Paleocene to early Oligocene Eyre Formation and in Early Cretaceous sediments (Stoian, 2010). Because of its location closer to the ranges and the Mount Painter domain basement, the potential Willawortina reservoir becomes smaller and is too small for providing enough uranium to the Four Mile deposit (Willawortina Formation 2, Table 6). The crystalline basement of the Mount Painter domain remains the only possible reservoir that could have provided enough uranium for the Four Mile mineralization.

Coming back to Beverley, the remaining reservoirs to consider are (1) the Mount Painter domain basement, (2) some exposed Four Mile mineralization upstream, and also (3) the Willawortina Formation. The geochronological data indicate that most of the uranium mineralization at Beverley predates the buildup of the Willawortina sequence. This therefore excludes this reservoir as a viable source of uranium. The absence of hydraulic interconnectivity between the Willawortina aquifers and the Beverley Sands aquifer also makes this source unlikely. In conclusion, the remaining possible sources for Beverley are the Mount Painter domain basement watershed, possibly with some component from the remobilization of Four Mile mineralization upstream.

Path of the mineralizing fluids

To account for the sudden increase in Cretaceous sedimentary component in the Namba Formation, it is necessary to consider a Miocene-Pliocene uplift, which exposed the Cretaceous formations present on the crystalline basement or simply enhanced the relief, permitting their partial reworking into the lake watershed. This uplift produced a flux inversion in the sedimentation at Beverley and a transition from lacustrine to littoral environment. This tectonic event produced some transpressive movements toward the northwest and faulting along a network of northeast-southwest subparallel faults. The Paralana High Plains are the final result of several basement compartment uplifts on the eastern side of the Paralana fault zone. The succession of uplifts along the faults under the Paralana High Plains has led to a progressive shoreline regression toward the east. The path of the fluids originating directly from the Mount Painter domain was either perpendicular to the fault directions (maximum dip) or channelized along the surface expression of the faults (Fig. 14). This interpretation means that the uranium from Beverley could come from the northwest (through Four Mile) or alternatively from the north-northeast, following the Poontana fault lineament. The Paralana High Plains substratum is schematically a stairs-like group of blocks (Fig. 14) and each of these blocks may have led to the formation of shoreline features in the Cenozoic formations.

The cross section in Figure 14 also shows the altitudes of Four Mile (+20 m) and Beverley (–30 m) orebodies, underlining the possibility of gravity-driven fluids crossing both deposits and precipitating their uranium in the appropriate environment. The thermoluminescence study of the quartz around Beverley complies with both possibilities, indicating that the sediments to the West of the Poontana fault have been in contact with mineralization (or mineralized fluids). The only data available to the north-northeast of Beverley also suggest an identical trend in this direction, indicating that part of the uranium at least came from this direction. The period of time required to form the Beverley ore cannot be determined exactly, but the geochronology data on carnotite may suggest at least 3 Ma.

Conclusions

The reconstitution of the genesis of the Beverley uranium deposit was made possible using a range of different techniques: heavy minerals assemblages from the ore and the nearby sediments, whole-rock and mineral geochemistry, and finally the integration of the regional geology to link the data collected at the deposit location.

The Beverley deposit is hosted in a detrital sandy formation (Beverley Sands) of Miocene age. The angular morphology of these quartz grains in the sands indicates a short transport of the sediments and deposition in a low-energy environment. The heavy minerals assemblage is incompatible with an origin in the local inliers only; the absence of corundum and the rarity of xenotime and monazite-(Ce) prove that the nearby outcropping crystalline basement was not the main source of sediments during the Miocene. Both typology and ages for Beverley Sands zircons also indicate a different, distal source. The presence of volcanic and granitic Cretaceous zircons (≥130 Ma), as well as Permo-Carboniferous zircons originating from S-type granitoids point to eastern Australia (New England orogen) as a source area. These materials were transported to the area by glaciers during the Cretaceous.

The mineralization at Beverley is mostly composed of coffinite with minor uraninite and associated native copper, pyrite, marcasite, carnotite, sphalerite, barite, and chalcopyrite. The presence of native lead necessitates highly reducing microenvironments ($f_{CH_{4(g)}} >> f_{CO_{2(g)}}$. Using the groundwater composition and the observed mineralogy, the prevailing conditions during the mineralization are estimated as: pH 6.3 to 8.4, with $\log f_{O_2}$ from –50 to –70 at 25°C. The reduction is essentially bacterial, as suggested by negative $\delta^{34}S$ in associated sulfides, bacteriomorph coffinite, the P contents of the coffinite nodules, and the limited amounts of organic matter in the main ore horizons. The high REE contents of the uranium ore and coffinite nodules are linked to an enriched source, but enrichment in intermediate REE may reflect the influence of Pliocene acid soil formation.

The upper part of the mineralization at Beverley has a different mineralogy, which records acidic oxidizing conditions (carnotite, no coffinite, alunite, kaolinite, goethite, gypsum). The prevailing conditions were between pH 3.9 and 4.5 and with $\log f_{O_2}$ from 0 to –30 at 25°C. This physicochemical environment of the Beverley Clays is interpreted to postdate the main mineralization and to result from the exposure of pyrite-rich mudstones to the surface by local uplift along fault structures (e.g., Poontana fault) in the Paralana High Plains.

The U-Pb ages obtained on coffinite and carnotite (6.7–3.4 Ma) indicate that the mineralization formed mostly, if not completely, prior to the Pliocene-Quaternary Willawortina

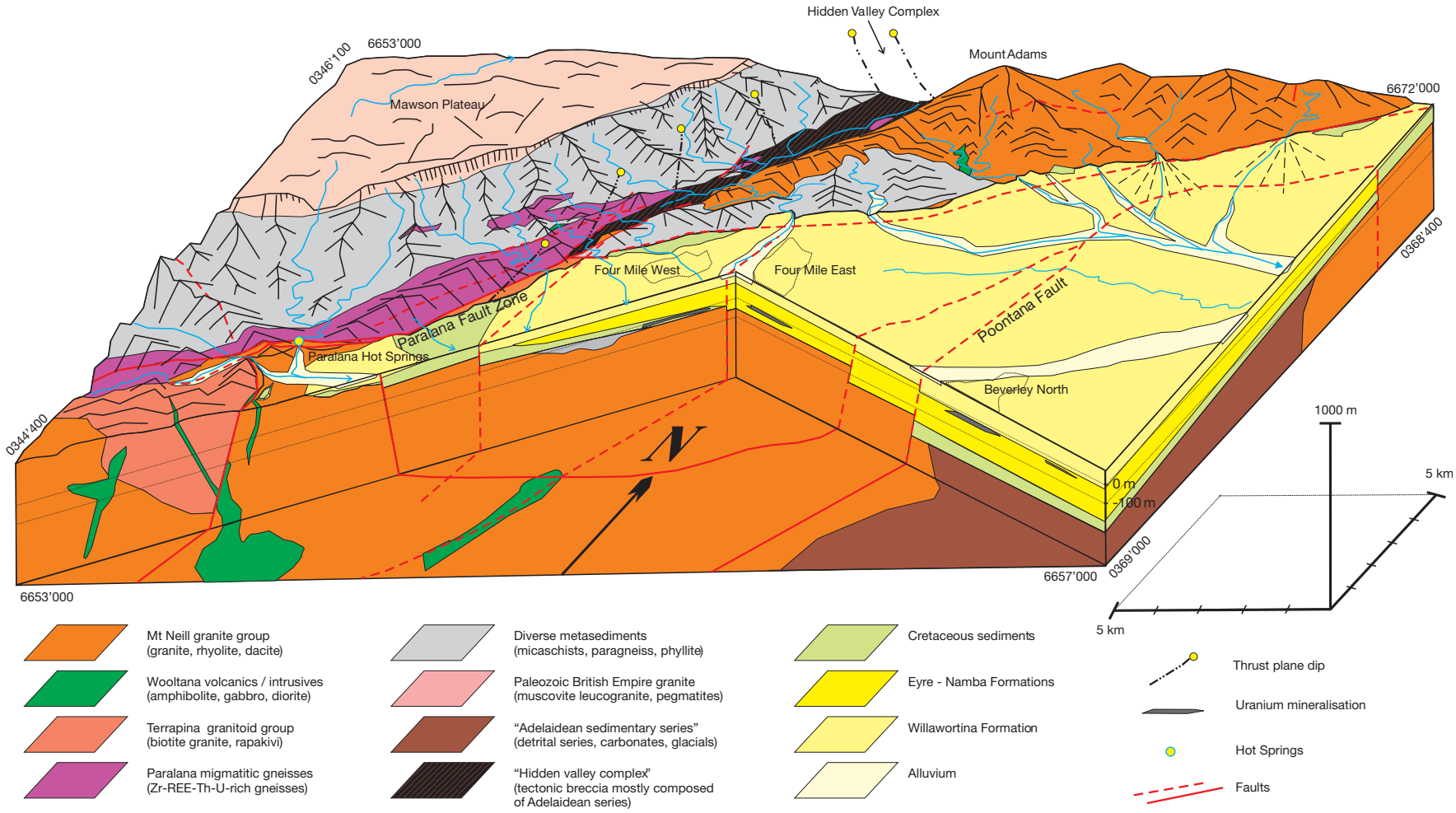

FIG. 14. Cross section and perspective projection of the Paralana High Plains to the Mount Painter domain. The geology reported is mostly inspired from the 1961 maps, with integration of new field information and the use of the radiometric (U) data to delimitate the migmatitic radioactive gneiss unit. The figure has been drawn at scale with a vertical exaggeration. Faults reported in the basement window are partly from Heathgate Resources data and from our own interpretation.

deposition (3.5–0.7 Ma). The three-dimensional setting favors two possible paths for uranium-bearing solutions toward Beverley: (1) from the Mount Painter domain through Four Mile deposit area and/or (2) along a north-northeast to south-southwest corridor following a paleoshoreline due to the uplift of the Paralana High Plains to the west. Geochronological, geochemical, mass-balance, and sedimentologic arguments indicate that the only possible uranium source is the Mount Painter domain basement.

The Beverley deposit has already proven its economic viability. Exploration around the mine, which led to the discovery of the Four Mile deposit, confirms the high potential of the Paralana High Plains district. The uranium sources in the Mount Painter domain can be considered as unlimited for providing uranium to the neighboring basins. Assuming only 10 percent U availability from a near-unconformity layer, the near-surface Mount Painter domain rocks from the Paralana High Plains watershed and the Willawortina Formation contain ~120,000 t U_3O_8. Similar settings (proximity to the Mount Painter domain, presence of post-Mesozoic faults, and presence of porous Cenozoic formation) can be found to the east of the Mount Neill-Mount Adams block, as well as to the north of the Mount Babbage inlier. If additional geochronological data on uranium mineralization could match the Pliocene age found at Beverley (e.g., at Four Mile), a precise reconstruction of the paleoenvironment around the Mount Painter domain at this time would bring a powerful tool to direct the future exploration, especially along paleolittoral features.

The sandstone-hosted Beverley uranium deposit can be classified in the tabular type according to the Bruneton and Cuney (2010) synthesis. The mineralization is primarily controlled by sedimentologic features which define the flat-shaped mineralized bodies. The deposit is however quite different from the Colorado Plateau-type mineralizations (absence of vanadium, more proximal setting), and more similar to the Arlit district deposits in Niger (similar ore grade, Precambrian basement proximity), although some differences occur (lacustrine origin of the Beverley Sands, age of the mineralization).

It is interesting to note that the economic value of uranium deposits in the province can be decided by sedimentologic features. Beverley is well suited for cost-effective in situ acid-leaching techniques mining because of its favorable hydrogeologic situation and because the host sediments have the right porosity and mineralogy (e.g., low carbonate and clay contents). At Beverley, these favorable sedimentologic features result from a very complex history, including lacustrine shores, high porosity, angular sands of ultimately glacial origin, and proximity to an active fault exposing basement rocks exceptionally rich in uranium.

Acknowledgments

This paper is based on the PhD research of the first author. It has been financed during the first three years through scholarships from the Australian International Postgraduate Research program and from CRC-LEME; the latter covered most of the analytical costs. We thank the Sprigg family for access to Arkaroola station and providing accommodation; Jean-Claude Lavanchy at the Centre d'Analyse Minérale in Lausanne for his technical support; Yann Lahaye for his support at the ICPMS; and Olivier Parize for his assistance at core logging. We are grateful to the team of the Adelaide Microscopy Centre, especially Angus Netting, Peter Self, and John Terlet for their assistance during the hundreds of hours spent in the Centre, Christophe Tenailleau for the X-ray diffraction treatment, and Jess Oram for his help in reviewing this work. The achievement of this research would not have been possible without the support of Heathgate Resources Pty. Ltd., who provided financial support through employment during the period 2007 to 2008. A special thanks to Geoff McConachy. The manuscript benefitted from the reviews of two anonymous reviewers and Larry Meinert.

REFERENCES

Alley, N.F., and Frakes, L.A., 2003, First known Cretaceous glaciation: Livingston Tillite Member of the Cadna-owie Formation, South Australia: Australian Journal of Earth Sciences, v. 50, p. 139–144.

Alpers, C.N., Rye, R.O., Nordstrom, D.K., White, L.D., and King, B.-S., 1992, Chemical, crystallographic and stable isotopic properties of alunite and jarosite from acid-hypersaline Australian lakes: Chemical Geology, v. 96, p. 203–226.

Bajo, C., Rybach, L., and Weibel, M., 1983a, Extraction of uranium and thorium from Swiss granites and their microdistribution. 1. Extraction of uranium and thorium: Chemical Geology, v. 39, p. 281–297.

——1983b, Extraction of uranium and thorium from Swiss granites and their microdistribution. 2. Microdistribution of uranium and thorium: Chemical Geology, v. 39, p. 299–318.

Bea, F., 1996, Residence of REE, Y, Th and U in granites and crustal protoliths: Implications for the chemistry of crustal melts: Journal of Petrology, v. 37, p. 521–552.

Belousova, E.A., Griffin, W.L., O'Reilly, S.Y., and Fisher, N.I., 2002, Igneous zircon: Trace element composition as an indicator of source rock type: Contributions to Mineralogy and Petrology, v. 143, p. 602–622.

Benbow, M.C., Callen, R.A., Bourman, R.P., and Alley, N.F., 1995, Tertiary: Deep weathering, ferricrete and silcrete, *in* Drexel, J.F., and Preiss, W.V., eds., The geology of South Australia: Adelaide, South Australia Geological Survey, p. 201–207.

Bethke, C.M., 1996, Geochemical reaction modelling, concepts and applications: New York, Oxford University Press, 414 p.

Bird, M.I., Andrew, A.S., Chivas, A.R., and Lock, D.E., 1989, An isotopic study of surficial alunite in Australia: 1. Hydrogen and sulfur isotopes: Geochimica et Cosmochimica Acta, v. 53, p. 3223–3237.

Blundy, J., and Wood, B., 2003, Mineral partitioning of uranium, thorium and their daughters, *in* Rosso, J.J., and Ribbe, P.H., eds., Uranium-series geochemistry: Washington, Mineralogical Society of America, p. 59–123.

Brugger, J., Krivovichev, S.V., Berlepsch, P., Meisser, N., Ansermet, S., and Armbruster, T., 2004, Spriggite, $Pb_3(UO_2)_6O_8(OH)_2(H_2O)_3$, a new mineral with β-U_3O_8–type sheets: Description and crystal structure: American Mineralogist, v. 89, p. 339–347.

Brugger, J., Long, N., McPhail, D.C., and Plimer, I., 2005, An active amagmatic hydrothermal system: The Paralana hot springs, northern Flinders Ranges, South Australia: Chemical Geology, v. 222, p. 35–64.

Brugger, J., Etschmann, B., Pownceby, M., Liu, W., Grundler, P. and Brewe, D., 2008, Tracking the chemistry of ancient fluids: Oxidation state of europium in hydrothermal scheelite: Chemical Geology, v. 257, p. 26–33.

Brugger, J., Meisser, N., Etschmann, B., Ansermet, N., and Pring, A., 2011, Paulscherrerite from the Number 2 Workings, Mt. Painter inlier, northern Flinders Ranges, South Australia: "Dehydrated schoepite" is a mineral after all: American Mineralogist, v. 96, p. 229–240.

Bruneton, P., and Cuney, M., 2010, L'uranium. 3. Géologie des principaux types de gisement : Géochronique, v. 113, p. 21–39.

Brunt, D.A., 1978, Uranium in Tertiary stream channels, Lake Frome area, South Australia: Australasian Institute of Mining and Metallurgy Proceedings, v. 266, p. 79–90.

Bryan, S.E., Ewart, A., Stephens, C.J., Parianos, J., and Downes, P.J., 2000, The Whitsunday volcanic province, Central Queensland, Australia: Lithological and stratigraphic investigations of a silicic-dominated large igneous province: Journal of Volcanology and Geothermal Research, v. 99, p. 55–78.

Burns, P.C., 1999, The crystal chemistry of uranium: Reviews in Mineralogy, v. 38, p. 23–90.

Burtt, A., Conor, C., and Robertson, S., 2004, Curnamona—an emerging Cu-Au province: MESA Journal, v. 33, p. 9–17.

Cai, C., Dong, H., Li, H., Xiao, X., Ou, G., and Zhang, C., 2007, Mineralogical and geochemical evidence for coupled bacterial uranium mineralization and hydrocarbon oxidation in the Shashagetai deposit, NW China: Chemical Geology, v. 236, p. 167–179.

Callen, R.A., 1975, The stratigraphy, sedimentology and uranium deposits of Tertiary rocks, Lake Frome area, South Australia: Unpublished M.Sc. thesis, Adelaide, Australia, University of Adelaide, 275 p.

Callen, R.A., and Tedford, R.H., 1976, New late Cainozoic rock units and depositional environments, Lake Frome area, South Australia: Royal Society of South Australia Transactions, v. 100, p. 125–167.

Callen, R.A., Alley, N.F., and Greenwood, D.R., 1995a, Tertiary: Interior non-marine basins—Lake Eyre basin, *in* Drexel, J.F., and Preiss, W.V., eds., The geology of South Australia: Adelaide, South Australia Geological Survey, p. 188–194.

Callen, R.A., Sheard, M.J., Benbow, M.C., and Belperio, A.P., 1995b, Quaternary: Alluvial fans and piedmont slope deposits, *in* Drexel, J.F., and Preiss, W.V., eds., The geology of South Australia: Adelaide, South Australia Geological Survey, p. 241–243.

Campana, B., Coats, R.P., Horwitz, R., and Thatcher, D., 1961a, 1:63'360 Gardiner sheet, Geological Atlas of South Australia: Department of Mines, Geological Survey of South Australia.

——1961b, 1:63,360 Moolawatana sheet, Geological Atlas of South Australia: Department of Mines, Geological Survey of South Australia.

Cardona, J.P.M., Mas, J.M.G., Bellón, A.S., Domínguez-Bella, S. and López, J.M., 2005, Surface textures of heavy-mineral grains: A new contribution to provenance studies: Sedimentary Geology, v. 174, p. 223–235.

Coats, R.P., 1973, Copley 1:250 000 Geological Map: Explanatory Notes: Adelaide, Department of Mines, Geological Survey of South Australia, 38 p.

Coats, R.P., and Blissett, A.H., 1971, Regional and economic geology of the Mount Painter province: Adelaide, A.B. James, Government Printer, Bulletin 43, 426 p.

Cojan, I., and Renard, M., 1997, Sédimentologie: Paris, Masson, 418 p.

Coleman, M.L., 1977, Sulphur isotopes in petrology: Journal of the Geological Society of London, v. 133, p. 593–608.

Curtis, J.L., Brunt, D.A., and Binks, P.J., 1990, Tertiary paleochannel uranium deposits of South Australia, *in* Hughes, F.E., ed., Geology of the mineral deposits of Australia and Papua New Guinea: Melbourne, Australian Institute of Mining and Metallurgy, p. 1631–1636.

De Caritat, P., and Kirste, D., 2005, Hydrogeochemistry applied to mineral exploration under cover in the Curnamona province: MESA Journal, v. 37, p. 13–17.

Dekov, V.M., Damyanov, Z.K., Kamenov, G.D., Bonev, I.K., and Bogdanov, K.B., 1999, Native copper and alpha-copper-zinc in sediments from the Adelaide geosyncline hydrothermal field (Mid-Atlantic Ridge, 26°N): Nature and origin: Marine Geology, v. 161, p. 229–245.

Draper, J.J., 1974, The geochemistry of Lake Frome, a playa lake in South Australia: BMR Journal of Australian Geology and Geophysics , v. 1, p. 83–104.

Elburg, M.A., Bons, P.D., Foden, J., and Brugger, J., 2003, A newly defined Late Ordovician magmatic-thermal event in the Mt. Painter province, northern Flinders Ranges, South Australia: Australian Journal of Earth Sciences, v. 50, p. 611–631.

Fanning, C.M., Teale, G.S., and Robertson, R.S., 2003, Is there a Willyama Supergroup sequence in the Mount Painter inlier?, *in* Peljo, M., ed., Broken Hill Exploration Initiative, 7–9 July 2003, Broken Hill, Australia, Geoscience Australia, p. 38–41.

Foden, J., Elburg, M.A., Dougherty-Page, J., and Burtt, A., 2006, The timing and duration of the Delamerian orogeny: Correlation with the Ross orogen and implications for Gondwana assembly: Journal of Geology, v. 114, p. 189–210.

Förster, H.-J., 2006, Composition and origin of intermediate solid solutions in the system thorite-xenotime-zircon-coffinite: Lithos, v. 88, p. 35–55.

Foster, D.A., Murphy, J.M., and Gleadow, A.J.W., 1994, Middle Tertiary hydrothermal activity and uplift of the northern Flinders Ranges, South Australia: Insights from the apatite fission-track thermochronology: Australian Journal of Earth Sciences, v. 41, p. 11–17.

Geisler, T., Pidgeon, R.T., Kurtz, R., van Bronswijk, W., and Schleicher, H., 2003, Experimental hydrothermal alteration of partially metamict zircon: American Mineralogist, v. 88, p. 1496–1513.

Goldhaber, M.B., Hemingway, B.S., Mohagheghi, A., Reynolds, R.L., and Northrop, H.R., 1987, Origin of coffinite in sedimentary rocks by sequential adsorption-reduction mechanism: Bulletin de Minéralogie, v. 110, p. 131–144.

Hansley, P.L., and Fitzpatrick, J.J., 1989, Compositional and crystallographic data on REE-bearing coffinite from the Grants uranium region, northwestern New Mexico: American Mineralogist, v. 74, p. 263–270.

Haynes, R.W., 1975, Beverley sedimentary uranium orebody, Frome embayment, South Australia: Australian Institute of Mining and Metallurgy (AusIMM) Monograph 5, p. 808–813.

Heathgate Resources Pty. Ltd., 1998, Beverley uranium mine, environmental impact statement: Adelaide, June 1998, Heathgate Resources Pty. Ltd., ISBN 0646357158.

Hochman, M.B.M., and Ypma, P.J.M., 1987, The accretionary migration of uranium in Tertiary sandstones—thermoluminescence evidence from the Beverley deposit, South Australia: Uranium, v. 3, p. 245–259.

Jackson, S.E., Pearson, N.J., Griffin, W.L., and Belousova, E.A., 2004, The application of laser ablation-inductively coupled plasma-mass spectrometry to in situ U-Pb zircon geochronology: Chemical Geology, v. 211, p. 47–69.

Jambor, J.L., and Roberts, A.C., 2000, New mineral names: Tongxinite: American Mineralogist v. 85, p. 263–266.

Janeczek, J., 1991, Composition and origin of coffinite from Jachymov, Czechoslovakia: Neues Jahrbuch für Mineralogie: Monatshefte 9, p. 385–395.

Jonsson, E., and Broman, C., 2002, Fluid inclusions in late-stage Pb-Mn-As-Sb mineral assemblages in the Långban deposit, Bergslagen, Sweden: Canadian Mineralogist, v. 40, p. 47–65.

Ker, D.S., ed., 1966, The hydrology of the Frome embayment in South Australia: Adelaide, Department of Mines of South Australia, Geological Survey, 98 p.

Klötzli, U.S., Koller, F., Scharbert, S., and Höck, V., 2001, Cadomian lower-crustal contributions to Variscan granite petrogenesis (South Bohemian pluton, Austria): Constraints from Zircon typology and geochronology, whole-rock, and feldspar Pb-Sr isotope systematics: Journal of Petrology, v. 42, p. 1621–1642.

Krieg, G.W., Alexander, E.M., and Rogers, P.A., 1995, Mesozoic: Jurassic-Cretaceous epicratonic basins: Eromanga basin, *in* Drexel, J.F., and Preiss, W.V., eds., The geology of South Australia. Adelaide: South Australia Geological Survey, p. 101–127.

Li, G., Peacor, D.R., Essene, E.J., Brosnahan, D.R., and Beane, R.E., 1992, Walthierite, $Ba_{0.5}Al_3(SO_4)_2(OH)_6$ and huangite, $Ca_{0.5}Al_3(SO_4)_2(OH)_6$, two new minerals of the alunite group from the Coquimbo region, Chile: American Mineralogist, v. 77, p. 1275–1284.

Long, D.T., Fegan, N.E., McKee, J.D., Lyons, W.B., Hines, M.E., and Macumber, P.G., 1992, Formation of alunite, jarosite and hydrous iron oxides in a hypersaline system: Lake Tyrell, Victoria, Australia: Chemical Geology, v. 96, p. 183–202.

Ludwig, K.R., 1979, Age of uranium mineralization in the Gas Hills and Crooks Gap districts, Wyoming, as indicated by U-Pb isotope apparent ages: ECONOMIC GEOLOGY, v. 74, p. 1654–1668.

Ludwig, K.R., and Grauch, R.I., 1980, Coexisting coffinite and uraninite in some sandstone-host uranium ores of Wyoming: ECONOMIC GEOLOGY, v. 75, p. 296–302.

Machel, H.G., Krouse, H.R., and Sassen, R., 1995, Products and distinguishing criteria of bacterial and thermochemical sulfate reduction: Applied Geochemistry, v. 10, p. 373–389.

Marsland-Smith, A., 2005, Geological setting and mineralogy of uranium mineralization at the Beverley deposit, Frome basin, SA, *in* Taylor, G.F., ed., 4th Sprigg Symposium, Uranium: Exploration, Deposits, Mines and Minewaste Disposal Geology, Glenside, 5 December 2005, South Australia, p. 18–19.

Martin, H.A., 1990, The palynology of the Namba Formation in the Wooltana-1 bore, Callabonna basin (Lake Frome), South Australia and its relevance to Miocene grasslands in central Australia: Alcheringa, v. 14, p. 247–255.

McConachy, G., McInnes, D., and Paine, J., 2006, Airborne electromagnetic signature of the Beverley uranium deposit, South Australia: Society of Economic Geologists Annual Meeting, 66th, New Orleans, Louisiana, Proceedings, p. 790–794.

McLennan, S.M., 1989, Rare earth elements in sedimentary rocks: Influence of provenance and sedimentary processes: Reviews in Mineralogy, v. 21, p. 169–200.

McLoughlin, S., 2001, The breakup history of Gondwana and its impact on pre-Cenozoic floristic provincialism: Australian Journal of Botany, v. 49, p. 271–300.

Mitchell, M.M., Kohn, B.P., O'Sullivan, P.B., Hartley, M.J., and Foster, D.A., 2002, Low-temperature thermochronology of the Mount Painter province, South Australia: Australian Journal of Earth Sciences, v. 49, p. 551–563.

Monecke, T., Dulski, P., and Kempe, U., 2007, Origin of convex tetrads in rare earth element patterns of hydrothermally altered siliceous igneous rocks from the Zinnwald Sn-W deposit, Germany: Geochimica et Cosmochimica Acta, v. 71, p. 335–353.

Nesbitt, H.W., 1979, Mobility and fractionation of rare earth elements during weathering of a granodiorite: Nature, v. 279, p. 206–210.

Neumann, N., 1996, Isotopic and geochemical characteristics of the British Empire Granite as indicators of magma provenance and processes of melt generation in the Mount Painter inlier, South Australia: Unpublished B.Sc. thesis, Adelaide, Australia, University of Adelaide, 38 p.

Neumann, N., Sandiford, M., and Foden, J., 2000, Regional geochemistry and continental heat flow: Implications for the origin of the South Australian heat flow anomaly: Earth and Planetary Science Letters, v. 183, p. 107–120.

Noble, R.J., Just, J., and Johnson, J.E., 1983, Catalogue of South Australian Minerals - 1983: Adelaide, D.J. Woolman, Government Printer, Handbook 7, 248 p.

Novgorodova, M.I., Tsepin, A.I., and Dmitriyeva, M.T., 1980, Zinc-rich variety of native copper: International Geology Review, v. 22, p. 1447–1450.

Potts, P.J., 1987, A handbook of silicate rock analysis: London, Academic and Professional, 622 p.

Pupin, J.-P., 1980, Zircon and granite petrology: Contributions to Mineralogy and Petrology, v. 73, p. 207–220.

Reid, A.J., Payne, J.L., and Wade, B.P., 2006, A new geochronological capability for South Australia: U-Pb zircon dating via LA-ICPMS: MESA Journal, v. 42, p. 27–31.

Rollinson, H., 1993, Using geochemical data: Evaluation, presentation, interpretation: Singapore, Longman Scientific and Technical, 352 p.

Rubatto, D., and Hermann, J., 2007, Experimental zircon/melt and zircon/garnet trace element partitioning and implications for the geochronology of crustal rocks: Chemical Geology, v. 241, p. 38–61.

Rubin, J.N., Henry, C.D., and Price, J.G., 1989, Hydrothermal zircons and zircon overgrowths, Sierra Blanca Peaks, Texas: American Mineralogist, v. 74, p. 865–869.

Sandiford, M., Hand, M., and McLaren, S., 1998, High geothermal gradient metamorphism during thermal subsidence: Earth and Planetary Science Letters, v. 163, p. 149–165.

Sawlowicz, Z., 1990, Native lead in the Polish Kupferschiefer: Neues Jahrbuch für Mineralogie: Monatshefte 8, p. 376–382.

Sircombe, K.N., 1999, Tracing provenance through the isotope ages of littoral and sedimentary detrital zircon, eastern Australia: Sedimentary Geology, v. 124, p. 47–67.

Stacey, J.S., and Kramers, J.D., 1975, Approximation of terrestrial lead isotope evolution by a two-stage model: Earth and Planetary Science Letters, v. 26, p. 207–221.

Stieff, L.R., Stern, T.W., and Sherwood, A.M., 1956, Coffinite, a uranous silicate with hydroxyl substitution—a new mineral: American Mineralogist, v. 41, p. 675–688.

Stoffregen, R.E., and Alpers, C.N., 1987, Woodhousite and svanbergite in hydrothermal ore deposits: Products of apatite destruction during advanced argillic alteration: Canadian Mineralogist, v. 25, p. 201–211.

Stoian, L.M., 2010, Palynology of Mesozoic and Cenozoic sediments of the Eromanga and Lake Eyre basins: Results from recent drilling in the northwest Frome embayment: MESA Journal, v. 57, p. 27–35.

Thode, H.G., and Monster, J., 1965, Sulfur isotope geochemistry of petroleum, evaporites and ancient seas: American Association of Petroleum Geologists Memoirs 4, p. 367–377.

Trudinger, P.A., Chambers, L.A., and Smith, J.W., 1985, Low-temperature sulfate reduction: Biological vs. abiological: Canadian Journal of Earth Sciences, v. 22, p. 1910–1918.

Van Achterbergh, E., Ryanm, C.G., and Griffin, W.L., 1999, GLITTER: Online interactive data reduction for the laser ablation ICP-MS microprobe [abs.]: Annual V. M. Goldschmidt Conference, 9th, 22–27 August 1999, Cambridge, Massachusetts, Abstract 7215, p. 305–306.

Veevers, J.J., 2006, Updated Gondwana (Permian-Cretaceous) earth history of Australia: Gondwana Research, v. 9, p. 231–260.

Warren, J.K., 2000, Evaporites, brines and base metals: Low-temperature ore emplacement controlled by evaporite diagenesis: Australian Journal of Earth Sciences, v. 47, p. 179–208.

Weeks, A.D., Coleman, R.G., and Thompson, M.E., 1959, Summary of the ore mineralogy: Geological Survey Professional Paper 320, p. 65–79.

Welch, S.A., Christy, A.G., Kirste, D., Beavis, S.G., and Beavis, F., 2007, Jarosite dissolution I—trace cation flux in acid sulfate soils: Chemical Geology, v. 245, p. 183–197.

Willner, A.P., Sindern, S., Metzger, R., Ermolaeva, T., Kramm, U., Puchkov, V., and Kronz, A., 2003, Typology and single grain U/Pb ages of detrital zircons from Proterozoic sandstones in the SW Urals (Russia): Early time marks at the eastern margin of Baltica: Precambrian Research, v. 124, p. 1–20.

Wilson, A., 1960, The microdetermination of ferrous iron in silicate minerals by a volumetric and colorimetric method: Analyst, v. 85, p. 823–827.

Wopfner, H., Callen, R.A., and Harris, W.K., 1974, The lower Tertiary Eyre Formation of the south-western Great Artesian basin: Journal of the Geological Society of Australia, v. 21, p. 17–52.

APPENDIX

TABLE A1. Heavy Minerals Assemblage in the WC2 Drill Core

Sample no.	Level (m)	Clay-silt	Tot. HM	NM	SM	MM	Carnotite	Coffinite	Copper	Barite	Sphalerite	Marcasite	Pyrite	Chalcopyrite	Rutile	Leucoxene	Zircon	Corundum	Anatase	"rutile index"
	Weight %						Detailed mineralogy of the NM fraction (% by grain counting)													
34	-1.5	18	0.164	0.006	0.011	0.147														
35	-8.6	63	0.594	0.038	0.110	0.446									61		30	9		2.0
36	-12.0	63	0.475	0.039	0.106	0.330									77		17	6		4.5
37	-12.6	57	0.570	0.043	0.102	0.425							2		45		50	3		0.9
38	-20.1	33	0.716	0.057	0.091	0.568									45		40	14	1	1.1
39	-25.5	31	1.029	0.055	0.111	0.863			<1					<1	50		36	13		1.4
40	-41.6	51	0.867	0.042	0.172	0.653														
41	-48.1	51	0.299	0.036	0.044	0.218									52		40	7	1	1.3
42	-51.7	19	0.169	0.052	0.014	0.104														
43	-61.0	42	0.837	0.153	0.162	0.522									65		28	6	1	2.3
44	-75.1	49	0.550	0.061	0.099	0.390									66	<1	30	3		2.2
45	-77.0	57	0.381	0.054	0.069	0.258														
46	-82.8	25	0.168	0.028	0.028	0.112							1		30		35	30		0.9
47	-84.2	29	0.466	0.073	0.083	0.310									55	1	33	10		1.7
48	-91.0	40	0.429	0.078	0.119	0.231														
49	-95.3	56	0.245	0.060	0.040	0.145									74		16	10		4.6
50	-97.1	41	0.021	0.006	0.007	0.007			3						80		6	6		13.3
51	-100.1	69	0.075	0.053	0.012	0.010			5						88	<1	3	3	1	29.3
52	-102.8	89	0.027	0.013	0.002	0.011			10	1					60	2	10	12		6.2
53	-104.9	73	0.027	0.009	0.002	0.015			<1	30					60		5	5		12.0
54	-105.5	97	0.001	0.000	0.000	0.001	1			<1					72	15	10	2		8.7
55	-110.1	94	0.006	0.001	0.001	0.004	<1								95	3	2	<1		49.0
56	-112.5	97	0.049	0.001	0.004	0.044	<1		<1						65	2	30	1	1	2.2
57	-115.6	92	0.003	0.001	0.001	0.002			1				<1		15	10	70	<1	3	0.4
58	-118.2	86	0.053	0.028	0.011	0.014									11	5	79	<1	4	0.2
59	-119.2	91	0.038	0.019	0.014	0.005									14	6	80		<1	0.3
60	-120.2	49	0.108	0.012	0.009	0.087	<1	<1	4				<1		8	8	75	<1	3	0.2
61	-121.2	65	0.106	0.046	0.042	0.018	<1		<1						5	8	85	<1	1	0.2
62	-122.9	55	0.083	0.048	0.035	0.000	<1								7	3	88	<1	1	0.1
63	-123.4	39	0.415	0.174	0.054	0.187				<1	<1				6	3	90		2	0.1
64	-125.6	77	0.023	0.001	0.002	0.020	2		<1	3	<1				40	<1	55	<1		0.7
65	-126.5	55	0.053	0.013	0.004	0.035	<1								20	4	75	1	<1	0.3
66	-127.4	80	0.054	0.028	0.025	0.002			<1			<1	<1		5	4	90	<1	1	0.1
67	-127.9	70	0.143	0.053	0.021	0.069	2		3	40	2	<1	1	<1	35	5	10	<1		4.0
68	-128.3	74	0.236	0.177	0.012	0.047	<1		<1	<1		6	35		5	4	48	<1	2	0.2
69	-128.6	66	0.318	0.231	0.035	0.052			<1			6	35	<1	5	4	48	<1	2	0.2
70	-130.0	86	0.294	0.250	0.023	0.021	<1		<1		<1	54	20	<1	2	1	12	<1		0.3
71	-131.1	93	0.026	0.011	0.003	0.011	3	8	2	3	2	5	25	1	20	2	30	<1		0.7
72	-131.2	89	0.197	0.182	0.004	0.011	3	8	2	3	2	5	25	1	20	2	30	<1		0.7
73	-132.0	97	0.791	0.771	0.003	0.016		92			3	2	3		<1		<1			
74	-132.4	98	0.010	0.009	0.000	0.001	5	15	<1	<1	<1	15	45	1	5	1	10			0.6
75	-132.6	93	0.115	0.101	0.005	0.009	5	15		5		15	45	1	5	1	10			0.6
76	-133.2	96	0.012	0.005	0.001	0.005	2	29		2	1	6	18		30	2	8	1		4.0
77	-135.0	99	0.003	0.001	0.001	0.001	1	30	23	<1	2	7	8		15	1	12	1		1.3

APPENDIX *(Cont.)*

TABLE A2. LA-ICP-MS U-Pb Zircon for WC2-63 (Beverley Sands)

													Apparent ages (Ma)								Retained ages (Ma)	
No.	Typology (subtypes)	Th (ppm)	U	U/Th	$^{207}Pb/^{206}Pb$	±	$^{206}Pb/^{238}U$	±	$^{207}Pb/^{235}U$	±	$^{208}Pb/^{232}Th$	±	$^{207}Pb/^{206}Pb$	±	$^{206}Pb/^{238}U$	±	$^{207}Pb/^{235}U$	±	$^{208}Pb/^{232}Th$	±	Age	Stratigraphic period
BE03z01	S24	115	99	0.860	0.05166	0.00309	0.02046	0.00036	0.14574	0.00856	0.00706	0.00017	270	132	131	2	138	8	142	3	130 ± 2.5	Cretaceous
BE01z03	P4 (vo)	60	58	0.963	0.05420	0.00387	0.02067	0.00040	0.15447	0.01079	0.00768	0.00024	379	153	132	3	146	9	155	5	130 ± 4	Cretaceous
BE02z24	S20	101	81	0.800	0.05107	0.00234	0.02119	0.00030	0.14922	0.00674	0.00682	0.00013	244	102	135	2	141	6	137	3	134 ±4	Cretaceous
BE02z07	P1 (vo)	303	280	0.924	0.04932	0.00258	0.02121	0.00036	0.14419	0.00745	0.00698	0.00016	163	118	135	2	137	7	141	3	135 ± 5	Cretaceous
BE01z14	S4 -S5 (vo)	120	111	0.926	0.05001	0.00268	0.02108	0.00034	0.14538	0.00765	0.00670	0.00016	195	120	135	2	138	7	135	3	135 ± 5	Cretaceous
BE02z26	S?	317	277	0.874	0.04997	0.00138	0.02140	0.00027	0.14746	0.00405	0.00678	0.00009	194	63	137	2	140	4	137	2	136 -3/+4	Cretaceous
BE02z06	S14	188	182	0.970	0.04965	0.00237	0.02234	0.00036	0.15292	0.00721	0.00740	0.00016	179	108	142	2	145	6	149	3	142 -5/+6	Cretaceous
BE01z07	D (vo)	87	104	1.193	0.05367	0.00241	0.03105	0.00047	0.22975	0.01017	0.01028	0.00024	357	98	197	3	210	8	207	5	196 -4/+5	Jurassic
BE02z04	P3	217	289	1.334	0.05208	0.00093	0.04055	0.00048	0.29110	0.00534	0.01292	0.00015	289	40	256	3	259	4	259	3	255 -5/+8	Permian
BE01z02	S23 -S24	39	60	1.545	0.05150	0.00268	0.04074	0.00065	0.28928	0.01482	0.01344	0.00040	263	115	257	4	258	12	270	8	257 ± 10	Permian
BE01z05	S12 -S13	51	79	1.527	0.05192	0.00430	0.04511	0.00100	0.32284	0.02619	0.01510	0.00069	282	178	284	6	284	20	303	14	284 ± 15	Permian
BE01z18	S24	145	185	1.274	0.05245	0.00139	0.04532	0.00058	0.32769	0.00873	0.01327	0.00021	305	59	286	4	288	7	267	4	286 ± 10	Permian
BE02z05	—	70	87	1.239	0.05734	0.00369	0.04634	0.00085	0.36641	0.02301	0.01488	0.00052	504	136	292	5	317	17	299	10	290± 9	Permian
BE01z08	—	255	346	1.358	0.05246	0.00117	0.04636	0.00057	0.33530	0.00755	0.01521	0.00021	306	50	292	4	294	6	305	4	293 ± 8	Permian
BE02z14	—	182	173	0.953	0.05267	0.00138	0.04663	0.00060	0.33860	0.00888	0.01475	0.00021	315	58	294	4	296	7	296	4	294 ± 9	Permian
BE01z17	—	68	51	0.744	0.05209	0.00412	0.04707	0.00099	0.33798	0.02620	0.01455	0.00046	289	170	297	6	296	20	292	9	296 ± 15	Permian
BE01z09	P1	215	200	0.930	0.05377	0.00174	0.04728	0.00064	0.35056	0.01126	0.01496	0.00025	361	71	298	4	305	8	300	5	297 ± 8	Permian
BE01z20	—	185	141	0.763	0.05463	0.00150	0.04714	0.00062	0.35501	0.00977	0.01469	0.00020	397	60	297	4	309	7	295	4	297 ± 8	Permian
BE02z27	S23	244	306	1.252	0.05334	0.00118	0.04751	0.00059	0.34938	0.00783	0.01477	0.00020	343	49	299	4	304	6	296	4	300 ± 8	Carboniferous
BE02z23	—	250	231	0.924	0.05373	0.00112	0.04833	0.00056	0.35807	0.00750	0.01529	0.00018	360	47	304	3	311	6	307	4	304 ± 8	Carboniferous
BE02z03	S20 -P4	219	161	0.732	0.05274	0.00122	0.04981	0.00063	0.36212	0.00851	0.01546	0.00019	318	52	313	4	314	6	310	4	304 ± 11	Carboniferous
BE03z02	—	230	168	0.732	0.05318	0.00136	0.04861	0.00062	0.35644	0.00914	0.01560	0.00020	337	57	306	4	310	7	313	4	306 ± 10	Carboniferous
BE02z10	J4	145	122	0.844	0.05350	0.00276	0.04947	0.00085	0.36462	0.01858	0.01579	0.00037	350	112	311	5	316	14	317	7	312 ± 14	Carboniferous
BE01z04	S23	478	490	1.025	0.05456	0.00153	0.04957	0.00066	0.37274	0.01047	0.01685	0.00026	394	61	312	4	322	8	338	5	313 ± 8	Carboniferous
BE01z15	—	208	239	1.149	0.05333	0.00144	0.05006	0.00064	0.36813	0.00995	0.01550	0.00024	343	60	315	4	318	7	311	5	315 ± 20	Carboniferous
BE01z06	—	155	145	0.939	0.05275	0.00159	0.05124	0.00067	0.37272	0.01117	0.01660	0.00025	318	67	322	4	322	8	333	5	323 ± 10	Carboniferous
BE02z19	—	305	302	0.991	0.05311	0.00102	0.05209	0.00060	0.38139	0.00738	0.01619	0.00019	333	43	327	4	328	5	325	4	327 ± 8	Carboniferous
BE01z01	P?	197	182	0.923	0.05429	0.00135	0.05960	0.00075	0.44609	0.01116	0.01935	0.00026	383	55	373	5	375	8	388	5	373 ± 11	Devonian
BE02z08	—	279	290	1.040	0.05711	0.00135	0.06439	0.00084	0.50687	0.01217	0.02080	0.00029	495	52	402	5	416	8	416	6	404 -8/+15	Devonian
BE01z12	—	174	164	0.940	0.05683	0.00144	0.06787	0.00086	0.53178	0.01350	0.02121	0.00030	484	55	423	5	433	9	424	6	424 ± 11	Silurian
BE02z09	S19 -S24	139	153	1.101	0.05628	0.00107	0.07006	0.00084	0.54351	0.01052	0.02104	0.00025	463	42	437	5	441	7	421	5	437 ± 12	Silurian
BE02z01	S12?	178	598	3.370	0.05667	0.00102	0.07056	0.00086	0.55143	0.01023	0.00932	0.00021	478	40	440	5	446	7	188	4	441 ± 11	Silurian
BE02z22	—	239	196	0.820	0.05693	0.00121	0.07357	0.00088	0.57745	0.01235	0.02242	0.00027	488	46	458	5	463	8	448	5	459 ± 11	Ordovician
BE02z02	S24?	104	128	1.235	0.05651	0.00170	0.07700	0.00107	0.59974	0.01805	0.02527	0.00044	472	65	478	6	477	11	505	9	478 ± 17	Ordovician
BE01z10	—	469	380	0.810	0.06242	0.00159	0.05431	0.00075	0.46733	0.01214	0.01847	0.00026	689	54	341	5	389	8	370	5	disc.	
BE01z11	—	237	264	1.113	0.06716	0.00323	0.05058	0.00083	0.46823	0.02198	0.01974	0.00051	843	97	318	5	390	15	395	10	disc.	
BE01z16	—	135	111	0.817	0.05838	0.00137	0.06758	0.00084	0.54383	0.01280	0.01931	0.00025	544	50	422	5	441	8	387	5	disc.	
BE01z19	—	249	181	0.725	0.05753	0.00238	0.04611	0.00071	0.36565	0.01497	0.01387	0.00026	512	89	291	4	316	11	278	5	disc.	
BE02z11	—	76	126	1.657	0.19461	0.00276	0.50573	0.00610	13.55286	0.19733	0.13587	0.00208	2782	23	2638	26	2719	14	2575	37	disc.	
BE02z12	—	272	245	0.902	0.06737	0.00127	0.06652	0.00075	0.61783	0.01152	0.02068	0.00024	849	39	415	5	489	7	414	5	disc.	
BE02z13	—	71	76	1.067	0.05784	0.00207	0.04614	0.00062	0.36796	0.01293	0.01478	0.00028	523	77	291	4	318	10	297	6	disc.	
BE02z15	—	254	312	1.230	0.06041	0.00089	0.07368	0.00084	0.61361	0.00935	0.02403	0.00026	618	32	458	5	486	6	480	5	disc.	
BE02z16	—	388	358	0.923	0.05776	0.00091	0.06783	0.00079	0.54017	0.00884	0.02107	0.00022	520	34	423	5	439	6	422	4	disc.	
BE02z17	—	65	81	1.245	0.06331	0.00199	0.06569	0.00088	0.57339	0.01777	0.02312	0.00041	719	65	410	5	460	11	462	8	disc.	
BE02z18	—	196	128	0.656	0.05748	0.00214	0.04489	0.00066	0.35568	0.01312	0.01405	0.00023	510	80	283	4	309	10	282	5	disc.	
BE02z20	—	658	397	0.604	0.09773	0.00158	0.20102	0.00260	2.70551	0.04678	0.05818	0.00067	1581	30	1181	14	1330	13	1143	13	disc.	
BE02z21	—	327	659	2.014	0.06353	0.00155	0.04948	0.00058	0.43336	0.01039	0.00955	0.00021	726	51	311	4	366	7	192	4	disc.	
BE02z25	—	667	359	0.538	0.06111	0.00211	0.01711	0.00023	0.14420	0.00489	0.00585	0.00008	643	72	109	1	137	4	118	2	disc.	

APPENDIX *(Cont.)*

TABLE A3. LA-ICPMS Isotopic Data for Coffinite and Carnotite

						Corrected isotopic ratios				1 sigma error				Ages and errors (Ma) (1 sigma) - indicative error related to common lead correction											
No.	Th (ppm)	U (ppm)	Th/U	Yield ratio $^{207}Pb/^{206}Pb$	Pb model age (Ga)	$^{207}Pb/^{206}Pb$	$^{206}Pb/^{238}U$	$^{207}Pb/^{235}U$	$^{208}Pb/^{232}Th$	$^{207}Pb/^{206}Pb$	$^{206}Pb/^{238}U$	$^{207}Pb/^{235}U$	$^{208}Pb/^{232}Th$	$^{207}Pb/^{206}Pb$			$^{206}Pb/^{238}U$			$^{207}Pb/^{235}U$			$^{208}Pb/^{232}Th$		
Coffinite – Beverley WC2																									
cof01	46	995448	0.0000	1.0130	0.00	0.1248	0.00013	0.00222	0.00379	0.0013	0.00001	0.00003	0.00004	2025	±18	(141)	±0.8	±0.1	(0.0)	2.3	±0.0	(0.2)	76	±1	(2078)
cof02	145	1026430	0.0001	1.0156	0.00	0.0782	0.00022	0.00237	0.00364	0.0008	0.00001	0.00003	0.00003	1151	±20	(156)	±1.4	±0.1	(0.0)	2.4	±0.0	(0.2)	73	±1	(676)
cof03	18	923608	0.0000	1.0174	0.00	0.0601	0.00034	0.00286	0.00463	0.0006	0.00001	0.00003	0.00005	609	±22	(160)	±2.2	±0.1	(0.0)	2.9	±0.0	(0.2)	93	±1	(5637)
cof04	175	1538763	0.0001	1.0120	0.00	0.0963	0.00014	0.00191	0.00372	0.0010	0.00001	0.00002	0.00003	1554	±19	(120)	±0.9	±0.1	(0.0)	1.9	±0.0	(0.1)	75	±1	(568)
cof05	23	1716439	0.0000	1.0201	0.00	0.0692	0.00021	0.00197	0.00461	0.0007	0.00001	0.00002	0.00004	904	±20	(119)	±1.3	±0.1	(0.0)	2.0	±0.0	(0.1)	93	±1	(4052)
cof06	1057	1347209	0.0008	1.0154	0.00	0.0726	0.00064	0.00640	0.00259	0.0007	0.00001	0.00008	0.00002	1004	±20	(44)	±4.1	±0.0	(0.0)	6.5	±0.1	(0.2)	52	±0	(98)
cof07	145	586259	0.0002	1.0177	0.00	0.0971	0.00017	0.00228	0.00304	0.0010	0.00001	0.00002	0.00003	1568	±19	(243)	±1.1	±0.1	(0.0)	2.3	±0.0	(0.3)	61	±1	(656)
cof08	76	1025206	0.0001	1.0159	0.00	0.1418	0.00006	0.00102	0.00331	0.0016	0.00001	0.00001	0.00004	2250	±19	(330)	±0.4	±0.1	(0.0)	1.0	±0.0	(0.2)	67	±1	(1401)
cof08b	314	960749	0.0003	1.0131	0.00	0.1575	0.00003	0.00069	0.00350	0.0018	0.00001	0.00001	0.00003	2429	±19	(445)	±0.2	±0.0	(0.0)	0.7	±0.0	(0.2)	71	±1	(308)
cof08c	41	607466	0.0001	1.0093	0.00	0.0672	0.00022	0.00199	0.00312	0.0007	0.00001	0.00002	0.00004	843	±22	(327)	±1.4	±0.0	(0.0)	2.0	±0.0	(0.3)	63	±1	(2316)
cof09	249	1334404	0.0002	1.0137	0.00	0.0583	0.00013	0.00104	0.00380	0.0006	0.00001	0.00001	0.00003	540	±22	(363)	±0.8	±0.0	(0.0)	1.1	±0.0	(0.2)	77	±1	(446)
cof10	319	1194741	0.0003	1.0174	0.00	0.0771	0.00004	0.00050	0.00311	0.0009	0.00001	0.00001	0.00003	1123	±22	(680)	±0.3	±0.0	(0.0)	0.5	±0.0	(0.2)	63	±1	(320)
cof10b	879	464343	0.0019	1.0150	0.00	0.0468	0.00105	0.00674	0.1186	0.0005	0.00001	0.00007	0.0009	37	±24	(152)	±6.8	±0.1	(0.0)	6.8	±0.1	(0.5)	2266	±17	(105)
Carnotite – Beverley WC2																									
carn01	31	399695	0.0001	1.0076	0.00	0.0464	0.00085	0.00542	0.5446	0.0005	0.00001	0.00006	0.0053	21	±24	(232)	±5.5	±0.1	(0.0)	5.5	±0.1	(0.6)	8788	±70	(2280)
carn02	90	1414164	0.0001	1.0168	0.00	0.0463	0.00066	0.00425	0.8618	0.0005	0.00001	0.00005	0.0079	13	±24	(96)	±4.3	±0.1	(0.0)	4.3	±0.1	(0.2)	12563	±86	(711)
carn03	37	339625	0.0001	0.9952	0.00	0.0462	0.00072	0.00457	0.2970	0.0005	0.00001	0.00006	0.0035	11	±25	(337)	±4.6	±0.1	(0.0)	4.6	±0.1	(0.7)	5256	±55	(2282)
carn04	67	661112	0.0001	1.0116	0.00	0.0464	0.00065	0.00418	0.5720	0.0005	0.00001	0.00005	0.0056	17	±24	(186)	±4.2	±0.1	(0.0)	4.2	±0.0	(0.3)	9143	±72	(1036)
carn05	25	1209663	0.0000	1.0069	0.00	0.0465	0.00055	0.00352	1.7686	0.0005	0.00001	0.00004	0.0221	22	±24	(130)	±3.5	±0.1	(0.0)	3.6	±0.0	(0.2)	20583	±161	(1720)
carn06	228	1166612	0.0002	1.0204	0.00	0.0462	0.00053	0.00336	0.0468	0.0005	0.00001	0.00004	0.0005	9	±24	(154)	±3.4	±0.1	(0.0)	3.4	±0.0	(0.2)	925	±9	(549)
carn07	25	740907	0.0000	0.9933	0.00	0.0463	0.00063	0.00402	1.3572	0.0005	0.00001	0.00005	0.0165	11	±25	(179)	±4.1	±0.1	(0.0)	4.1	±0.0	(0.3)	17331	±142	(2035)
carn08	283	1530451	0.0002	1.0066	0.00	0.0467	0.00079	0.00508	0.1377	0.0005	0.00001	0.00007	0.0014	35	±24	(79)	±5.1	±0.1	(0.0)	5.1	±0.1	(0.2)	2608	±25	(377)
carn09	242	1130958	0.0002	1.0200	0.00	0.0466	0.00069	0.00442	0.1237	0.0005	0.00001	0.00006	0.0012	29	±24	(125)	±4.4	±0.1	(0.0)	4.5	±0.1	(0.2)	2358	±21	(492)

TABLE A4. Whole-rock Chemical Composition of the Sediments in WC2

Formation	Willawortina		Namba							
Sample no.	964	966	967	968	969	971	972	974	976	978
Level (m)	–35 m	–84 m	–98 m	–106 m	–111 m	–120 m	–127 m	–130 m	–132 m	–135 m
Major and minor elements (wt %)										
SiO_2	63.76	79.59	75.17	58.90	52.05	81.38	82.13	59.19	59.27	59.18
TiO_2	0.71	0.36	0.66	1.05	0.73	0.75	0.91	0.60	1.11	0.77
Al_2O_3	16.80	9.32	13.80	19.36	26.27	9.40	10.15	20.53	23.03	17.78
Fe_2O_3	4.62	2.48	1.21	5.30	3.99	2.31	0.88	5.92	2.55	7.98
FeO	0.40	0.50	0.40	0.20	0.10	0.40	0.20	0.10	0.70	0.30
MnO	0.02	0.03	0.01	0.01	0.00	0.01	0.01	0.01	0.01	0.02
MgO	2.56	0.74	0.61	1.35	0.54	0.35	0.27	1.18	0.79	2.47
CaO	0.54	0.25	0.20	0.72	0.35	0.18	0.15	0.70	0.43	0.81
Na_2O	1.49	0.99	0.70	0.69	0.42	0.34	0.33	0.60	0.39	0.66
K_2O	3.31	2.59	2.58	1.74	1.38	0.95	0.97	0.68	0.83	1.60
P_2O_5	0.05	0.05	0.05	0.23	0.19	0.07	0.08	0.14	0.06	0.06
UO_2	0.00	0.00	0.00	0.01	0.01	0.00	0.00	0.01	*0.99	0.00
BaO	0.05	0.04	0.04	0.06	0.04	0.04	0.04	0.03	0.02	0.04
ZrO_2	0.04	0.03	0.05	0.03	0.02	0.04	0.05	0.02	0.03	0.02
Rb_2O	0.03	0.02	0.02	0.02	0.01	0.01	0.01	0.01	0.03	0.04
SrO	0.01	0.01	0.01	0.20	0.18	0.03	0.05	0.14	0.01	0.04
ZnO	0.01	0.00	0.00	0.01	0.00	0.00	0.00	0.00	0.01	0.03
Co_2O_3	0.01	0.03	0.03	0.00	0.00	0.02	0.02	0.00	0.00	0.00
V_2O_5	0.01	0.01	0.01	0.02	0.02	0.01	0.01	0.02	0.04	0.03
LOI	5.35	2.38	4.00	9.58	13.46	3.55	3.29	9.76	8.96	7.99
S	0.24	0.06	0.86	**1.28	**2.35	0.15	0.17	0.65	0.21	0.00
Sum	99.77	99.42	99.55	99.48	99.76	99.84	99.55	99.64	99.26	99.82
Trace elements (ppm)										
Ba	410	377	371	559	349	327	344	258	159	378
Rb	310	167	190	198	52	47	49	60	263	333
Sr	109	64	52	1655	1502	257	461	1167	110	180
*Y	61.7	63.4	57.9	19.5	8.0	14.6	16.7	7.4	120.5	144.2
Ni	12	7	6	8	4	7	6	6	28	*49
Cu	54	24	17	88	23	18	16	43	42	30
Zn	56	34	35	75	21	37	27	38	101	239
*Pb	15.9	20.3	18.0	80.8	19.1	9.9	10.8	28.1	41.6	15.0
Ga	25	15	21	31	19	12	12	12	26	<10
V	60	48	30	124	94	76	65	103	236	170
Sc	19	8	8	40	31	9	8	35	24	* 20
Cr	35	23	23	57	111	50	48	76	109	* 74
*As	<1.9	4.1	<3.8	3.2	5.2	<2.4	<2.6	<1.5	2.7	6.6
*Mo	1.23	1.85	2.94	6.19	1.03	2.55	1.14	2.90	9.20	1.04
Zr	290	223	336	230	120	265	336	125	198	130
*Nb	30.69	19.58	33.59	34.51	10.05	10.11	9.38	9.11	14.31	9.89
*Hf	8.09	6.22	8.74	5.77	3.25	7.60	8.94	3.78	3.92	3.76
*Ta	3.64	4.25	5.13	3.11	0.85	2.51	1.89	1.02	0.85	0.93
Th	40	38	18	37	8	15	7	18	* 19	28
*U	10.1	7.2	11.4	49.3	29.2	28.2	6.9	50.9	8771	9.0
*La	103.23	104.62	92.50	60.71	25.00	39.88	112.69	33.28	44.47	67.32
*Ce	157.64	160.07	153.27	65.14	34.87	63.59	122.05	30.52	125.56	157.29
*Pr	18.13	18.70	15.44	5.90	3.22	5.35	8.54	2.07	21.01	18.62
*Nd	63.39	67.06	52.29	19.02	9.59	18.35	24.75	6.24	96.47	82.80
*Sm	9.76	9.74	8.72	3.81	1.53	3.51	3.44	1.17	26.04	15.77
*Eu	1.28	1.17	0.72	0.53	0.26	0.35	0.35	0.24	4.09	2.85
*Gd	9.64	11.38	7.07	3.61	1.54	2.46	3.17	0.88	20.98	20.08
*Tb	1.35	1.97	1.02	0.50	0.15	0.32	0.50	0.20	3.76	3.31
*Dy	10.00	11.33	11.52	3.28	1.42	2.28	4.00	1.03	22.19	22.41
*Ho	2.34	2.64	1.77	0.72	0.17	0.51	0.71	0.36	4.35	5.30
*Er	5.64	6.10	5.34	2.58	0.81	1.45	1.78	1.03	11.03	16.87
*Tm	0.93	1.05	1.19	0.27	<0.07	0.40	0.25	0.18	1.37	2.38
*Yb	5.54	5.90	7.69	2.94	0.79	1.31	2.46	1.05	10.52	16.14
*Lu	1.07	0.96	0.98	0.40	0.21	0.23	0.42	0.12	1.46	2.47
Σ REE	390	403	360	169	80	140	285	78	393	434
% lREE	87.8	87.0	87.2	89.0	91.4	90.8	94.0	92.0	73.1	75.2
% *m*REE	8.2	8.8	8.1	6.9	6.2	6.4	4.0	4.5	19.6	14.9
% *h*REE	4.0	4.1	4.7	4.1	2.5	2.8	2.0	3.5	7.3	10.0
Fe^{2+}/Fe^{3+}	0.10	0.22	0.37	0.04	0.03	0.19	0.25	0.02	0.31	0.04

The heavy minerals have been listed in the column with the authigenic species first, followed by the detrital ones; the reported percentage is evaluated by grain counting in the NM (non-magnetic) fraction; the percentage of clay to very fine sands corresponds to the washout loss from panning, after drying and weighing of the remaining fractions; a total of 37.21 g of HM has been recovered from WC2

* = ICPMS data

** = Sulfur as SO_3